MULTIDECADAL TRENDS IN NEARSHORE SEDIMENT TRANSPORT AND MORPHODYNAMICS ALONG THE EASTERN COAST OF LAKE MICHIGAN: IMPLICATIONS FOR BEACH RECOVERY FOLLOWING HIGH LAKE LEVELS

By

Nathaniel Hunter Penrod

A THESIS

Submitted to
Michigan State University
in partial fulfillment of the requirements
for the degree of

Geography—Master of Science

2023

ABSTRACT

Coastal erosion is a ubiquitous hazard for sandy beaches in the Laurentian Great Lakes, especially during periods of more energetic wave climates associated with high lake levels. A fundamental barrier to managing these hazards is the lack of a process-based, quantitative understanding of longshore and cross-shore sediment exchange and connectivity across the entire coastal profile. In this study, a unique multidecadal dataset of beach and nearshore profiles collected at six sandy beaches along the eastern coast of Lake Michigan and contemporaneous hydrodynamic data are utilized to quantitatively identify long-term boundaries of sediment transport zones during accretionary and erosive wave conditions. Data analysis demonstrates that accretionary wave conditions can transport sediment onshore nearly exclusively from the lower reaches of the subaerial beach and from shallow sediment ridges in the inner nearshore while erosive wave conditions can mobilize sediment from all areas of the profile and redistribute it offshore. While sediments stored in deeper nearshore bars in the surf zone are activated by high-energy erosive wave conditions, they likely only function as multidecadal sinks for eroded beach sediment and not as sources of sediment for near-term beach accretion. The results of this study also demonstrate that cross-shore sediment transport has a more dominant role in long-term profile morphology change than longshore sediment transport along this stretch of coastline. Most importantly, the findings of this study suggest that future rates of beach recovery following high lake levels are likely to decrease in the study region as extensive coastal armoring will reduce sediment availability in the narrow profile zones activated during accretionary conditions. By identifying the edges of active sediment transport zones during accretionary and erosive wave conditions, this study is an initial step towards being able to better forecast the likelihood and manage the impacts of coastal erosion and beach recovery in the future.

This thesis is dedicated to my family, especially to Mom and Dad.
I will always be grateful for your love, encouragement, and support during this season of my life.

ACKNOWLEDGEMENTS

I would like to extend special thanks to my graduate advisor and thesis committee chair, Dr. Ethan Theuerkauf, for his thoughtful guidance and patient mentorship over the past two years. Collaborating with him on this thesis research project has been instructive and incredibly rewarding.

I would also like to extend gratitude to my thesis committee members, Dr. Erin Bunting and Dr. Alan Arbogast, for their comments and feedback which improved the quality of this thesis.

I would like to thank Dr. Guy Meadows, Dr. Lorelle Meadows, and other members of the Ocean Engineering Laboratory at the University of Michigan for sharing their coastal profile survey data collected between 1988 and 2000. I would also like to thank Sarah Grace Lott and Clyde Bunting from the Coastal Processes and Geomorphology Laboratory at Michigan State University for their fieldwork surveying coastal profiles during the 2021 field season. Without these datasets this study would not have been possible.

TABLE OF CONTENTS

LIST OF TABLES vi

LIST OF FIGURES vii

LIST OF ABBREVIATIONS viii

Introduction 1

Study Area and Methods 18

Results 37

Discussion 53

Conclusion 60

REFERENCES 62

APPENDIX A: WAVE INFORMATION STUDY STATION INFORMATION 77

APPENDIX B: EXAMPLE OF CLIPPED COASTAL PROFILES 78

APPENDIX C: PROFILE SECTOR AND SUBSECTOR CLASSIFICATION 79

APPENDIX D: MEAN SEDIMENT MOBILIZATION LIKELIHOOD 81

LIST OF TABLES

Table 1. *Study site descriptions.* 20

Table 2. *Profile interpolation accuracy assessment results.* 37

Table 3. *Summary of changes in coastal profile area, 1988 – 2021.* 39

Table 4. *Averaged wave parameters and active zone limits for AC, ME, and SE MCs.* 43

Table 5. *Average wave directions and velocities associated with trends in LS/CS sediment transport.* 47

Table 6. *Wave Information Study (WIS) station information.* 77

LIST OF FIGURES

Figure 1. *Lake Michigan monthly mean lake level elevations from 1980 – 2021.* 9

Figure 2. *Diagram of coastal profile morphology sectors and processes*.....12

Figure 3. *Study area map.* 19

Figure 4. *Examples of classification of cross-shore profile sectors at UM04 and UM14 based on standard deviations of profile elevations.* 27

Figure 5. *Calculating change in profile area*. 28

Figure 6. *LvC index.* 29

Figure 7. *Changes in beach and nearshore profile areas, 1988 – 2021.* 40

Figure 8. *Monthly variations in morphodynamic conditions, wave height, and lake level.* 44

Figure 9. *Profile LvC index values, 1988 – 2021.* 46

Figure 10. *Average wave vectors under different morphodynamic conditions.* 48

Figure 11. *Mean sediment mobilization likelihoods by profile sector.* 51

Figure 12. *UM04 mean sediment mobilization likelihood and active sediment transport zones, 2021.* 52

Figure 13. *Example of unclipped and clipped profile extents from UM14.* 78

Figure 14. *Classification of cross-shore profile sectors based on standard deviations of profile elevations.* 79

Figure 15. *Mean sediment mobilization likelihood across all study sites*. 81

LIST OF ABBREVIATIONS

AC	Accretionary morphodynamic condition
CS	Cross-shore
DOC	Depth of closure
DOC_e	Effective depth of closure
H_e	Effective wave height, highest 0.137% of observed waves
H_s	Significant wave height, average of the highest third of observed wave heights
LS	Longshore
MC	Morphodynamic condition
ME	Moderately erosive morphodynamic condition
R_2	Wave runup, highest 2% of wave runup peaks
$R_{2,\,e}$	Effective wave runup, highest 2% of wave runup peaks during the highest 0.137% of observed wave heights
RMSE	Root mean square error
SE	Severely erosive morphodynamic condition
T_e	Peak spectral wave period associated with the effective wave height
T_p	Peak spectral wave period

Introduction

Coastal erosion and accretion are complex processes resulting from gradients in longshore (LS) and cross-shore (CS) sediment transport induced by local and regional wave and water level dynamics. In the Laurentian Great Lakes, a wide range of fluctuations in mean lake levels pose a unique challenge to mitigating the hazardous impacts of erosion. Periods of high lake levels are linked with more energetic wave climates and heightened storm activity (Huang et al., 2021; Meadows et al., 1997) which result in increased rates of shoreline erosion (Birkemeier, 1981; Hands, 1976; Theuerkauf et al., 2019). Greater rates of coastal erosion during high lake levels cause billions of dollars of damage (Angel, 1995) and often lead to the wide-spread construction of shoreline armoring to slow the immediate impacts of erosion (Dobie et al., 2022; House, 2020; Lino Grima, 1993; Rovey & Borucki, 1994). During the most recent rise and peak in high lake levels between 2013 and 2020, areas of the Great Lakes experienced enhanced rates of shoreline recession (Troy et al., 2021), severe foredune erosion (Kilibarda & Kilibarda, 2022), accelerated loss of coastal habitat (Theuerkauf & Braun, 2021), and the destruction and landward migration of coastal wetlands (Anderson et al., 2023).

While the processes and dominant offshore sediment transport characteristic of erosive conditions have been well studied and can be modeled with some reliability (Dubarbier et al., 2015; Eichentopf et al., 2018; Gallagher et al., 1998; Hoefel & Elgar, 2003), the accretionary processes which lead to beach recovery remain poorly quantitatively constrained and cannot be reliably numerically modeled at present (Aagaard et al., 2002; Grossmann et al., 2022; Kobayashi & Jung, 2012; Ruggiero et al., 2009; Sanchez-Arcilla & Caceres, 2018; van Rijn et al., 2011; Volpano et al., 2022). The lack of model reliability for beach accretion is primarily due to the relative scarcity of field and laboratory observations of beach accretion at high degrees of

temporal resolution which would allow for the development of more accurate parameterizations of coastal processes (Eichentopf et al., 2018; van Rijn et al., 2011). Consequently, it is incredibly challenging to predict when or if sediment transported offshore during beach erosion will be returned to the beach. Given the inherent vulnerability of Great Lakes coasts to accelerated erosion during periods of high lake level, it is imperative that coastal managers and property owners be able to effectively mitigate risks posed by erosion and predict the manner and possibility of subsequent beach recovery.

There are several obstacles to improving the quantitative understanding of beach erosion and accretion in the Great Lakes. A primary and fundamental challenge is the lack of long-term (multidecadal or longer) data sets which are required to effectively assess the impacts of multiple morphodynamic cycles (Gorman et al., 1998; López et al., 2020; Splinter et al., 2013; Splinter & Coco, 2021; Zuzek et al., 2003). Previous research of coastal geomorphic change in the Great Lakes has largely been conducted over timescales which do not encompass multiple cycles of rising and falling lake levels and primarily focuses on periods of rising water levels. For instance, previous studies have analyzed coastal morphological change and sediment transport during storm events (Aagaard & Greenwood, 1995; Greenwood et al., 2006; Houser & Greenwood, 2005a), over several months or seasons (Boczar-Karakiewicz & Davidson-Arnott, 1987; Davis & Fox, 1972; Dubois, 1973; Farhadzadeh et al., 2018; Fox & Davis, 1973; Houser & Greenwood, 2005b; Volpano et al., 2020, 2022), over several years (Bajorunas & Duane, 1967; Davis, 1976; Hands, 1976, 1984; Saylor & Hands, 1970; Tanner, 1975; Theuerkauf et al., 2019; Troy et al., 2021; Weishar & Wood, 1983; Wood & Weishar, 1984), and occasionally over a decade or more (Hands, 1979, 1980; Stockberger & Wood, 1991; Wood, 1988).

However, only recent work such as that by Theuerkauf et al. (2022), Mattheus et al. (2022), and Abdelhady and Troy (2023) have begun to address multidecadal changes in coastal profile morphology in the Great Lakes which span multiple cycles of rising and falling lake levels. These types of studies are essential, as previous studies have shown that it is usually impossible to scale up the findings of localized, deterministic observations of sediment transport and wave dynamics to explain morphological change over larger spatial scales and time periods (Aagaard et al., 2004; M. Larson & Kraus, 1995; Pape et al., 2010; Pilkey & Cooper, 2002; Ruessink et al., 1998).

Another barrier to understanding beach recovery is poor quantitative understanding of the morphodynamic processes that lead to beach accretion. The hypothesis that calm, non-breaking wave conditions generally lead to onshore-directed sediment transport and beach accretion is widely accepted in the literature (Aubrey, 1979; Davis, 1976; Elfrink & Baldock, 2002; Fox & Davis, 1973; Grossmann, Hurther, van der Zanden, et al., 2023; Hallermeier, 1981; Hands, 1980; Ruessink & Terwindt, 2000; Sunamura & Horikawa, 1974). Usually, the process of beach accretion and gradual shoreline progradation begins with the shoreward transport of sediment stored in shallow bars or storm ridges just offshore of the shoreline where calm wave conditions can activate and suspend fine-grained sediment particles (Evans, 1939; Hands, 1984; Houser, 2009; Morton et al., 1994; M. S. Phillips et al., 2015, 2017). These shallow bars or sediment ridges should not be confused with nearshore bars, sometimes referred to as longshore bars, which contain much larger volumes of sediment and occur along deeper portions of the profile in the surf zone (see Figure 2b). Although some conceptual models based upon wave and sediment characteristics have been proposed to help classify calm, accretionary beach states (Short, 1979;

Wright et al., 1985; Wright & Short, 1984), the quantitative definition of "calm" wave conditions appears to be relative to a given beach or study.

Furthermore, there is a lack of a clear definition of the meaning of the term "beach recovery." Beach recovery can be defined in terms of losses or gains in sediment or as a return to pre-storm positions of key morphological features such as the shoreline and nearshore bar crests (Morton et al., 1994). However, recovery is highly site-specific and can vary in what it looks like and how long it takes (Corbella & Stretch, 2012). For the purposes of this study, beach recovery is defined in terms of sediment gain following periods of beach erosion. This definition was selected to avoid confusing the effects of shoreline retreat associated with inundation during high water levels and actual sediment erosion. Previous work in the Great Lakes demonstrated that rising lake levels account for 20-26% of measured shoreline retreat, while the remaining 74-80% of measured shoreline retreat was directly attributable to sediment erosion during high lake levels (Dubois, 1975; Hands, 1976). While beaches may still become wider during periods of low lake level, beaches remain more vulnerable to future erosion if sediment is not regained through accretion following accelerated periods of erosion during high lake levels.

Another obstacle to predicting beach erosion and accretion is the inherent complexity and site-specific nature of sediment transport and the resulting morphology change. Sediment transport exhibits high spatiotemporal variability (Aagaard & Greenwood, 1994; Zuzek et al., 2003) and is the outcome of the interaction of a complex array of morphodynamic variables (Bird, 1983; Osborne & Greenwood, 1992; Pilkey & Cooper, 2002; Pranzini & Williams, 2021). Higher volumes of both LS and CS sediment transport are typically associated with storm activity (Davis, 1976; Lick et al., 1994; Mortimer, 1988), although the episodic nature of sediment transport makes study results highly time-scale dependent (M. Larson & Kraus, 1995;

Ruessink et al., 1999). Additionally, human modification of the coast, especially through shoreline armoring and the construction of harbor breakwaters and jetties can substantially alter the gradients of LS and CS sediment transport by reducing sediment volumes transported via littoral drift and how wave energy is dissipated at the shoreline (Bajorunas & Duane, 1967; Kittinger & Ayers, 2010; Lin & Wu, 2014; Lino Grima, 1993; Morisawa & King, 1974; Saylor & Hands, 1970; Wood, 1988). A further complicating factor is the lack of knowledge of the long-term relationship between the relative dominance of LS and CS sediment transport processes (López-Dóriga & Ferreira, 2017). While changes in LS transport are typically linked to long-term changes in profile and shoreline morphology (Ashton & Murray, 2006; Roelvink & Brøker, 1993), CS transport processes are responsible for many of the most observable and dramatic changes in profile morphology such as the offshore transfer of beach and dune sediments to the inner nearshore during storms (Hands, 1984; Olson, 1958; Thom & Hall, 1991; van Dijk, 2021), and the genesis, migration, and growth or decay of nearshore bars (Aagaard et al., 2008; Dyhr-Nielsen & Sørensen, 1970; Greenwood et al., 2006; Houser & Greenwood, 2007; Marinho et al., 2020).

Finally, and perhaps most essentially, it is difficult to predict beach accretion because there are few quantitative assessments of the degree of sediment connectivity across the entire beach and nearshore profile at multidecadal timescales (Aagaard, 2014). Sediment connectivity describes how sediment is transported and exchanged between different sections of beach and nearshore morphology (Anthony & Aagaard, 2020). While the near-term (weeks to months) relationship between beach recovery and the transport of shallow nearshore sediments has been demonstrated (Fox & Davis, 1973; Morton et al., 1994; M. S. Phillips et al., 2017), it remains poorly quantitatively constrained over longer timescales. Furthermore, patterns of potential long-

term sediment transport between nearshore bars and the subaerial beach are not well quantified. While observations of the variability of nearshore bar CS position and volume led previous researchers to speculate about a potential mechanism of onshore sediment transfer from these nearshore bars to the subaerial beach (e.g. Bajorunas & Duane, 1967), field observations have not been able to quantitatively confirm the degree of potential onshore sediment transport from nearshore bars to the subaerial beach.

Subaerial beach erosion and accretion are often the most visible components of sediment exchanges across and along beach and nearshore profiles and thus receive the most amount of attention from the general public (Hands, 1980; Lino Grima, 1993). However, beaches are just one component of a multifaceted morphodynamic system which involves complex interactions and feedbacks between water motion, sediment transport, and underlying morphology (King, 1970; Wijnberg & Kroon, 2002). Previous studies in the Great Lakes have investigated the impacts of wave action and changing water levels on coastal bluff recession (Amin & Davidson-Arnott, 1995; Krueger et al., 2020; Rovey & Borucki, 1994; Vallejo & Degroot, 1988; Volpano et al., 2020), dune and foredune erosion and accretion (Arbogast et al., 2023; Arbogast & Loope, 1999; Davidson-Arnott & Bauer, 2021; Olson, 1958; Olyphant & Bennett, 1994; van Dijk, 2021), shoreline recession and beach erosion (Abdelhady & Troy, 2023; Fox & Davis, 1973; Mattheus et al., 2019, 2022; Theuerkauf et al., 2019; Troy et al., 2021; Wood & Weishar, 1984), and the cross-shore migration of nearshore bars (Bajorunas & Duane, 1967; Davidson-Arnott, 1988; Davis, 1976; Davis & Fox, 1972; Greenwood et al., 2006; Hands, 1976; Houser & Greenwood, 2005a; Saylor & Hands, 1970; Theuerkauf et al., 2022). Despite these investigative efforts, a quantitative understanding of the sediment connectivity between different profile sections, especially nearshore bars and the subaerial beach, remains underdeveloped.

To begin to address these current knowledge gaps, this study utilizes a unique dataset of beach and nearshore profile observations collected using various methods between 1988 and 2021 (Norton et al., 2011; Theuerkauf et al., 2022) and contemporaneous records of lake level and wave conditions to examine multidecadal trends in profile morphology at six sandy beaches along the eastern shore of Lake Michigan. The shoreline of this region is primarily composed of unconsolidated, fine-grained sediments which form pristine sandy beaches, striking bluffs, and some of the largest freshwater dunes in the world (Arbogast et al., 2023; G. Larson & Schaetzl, 2001). The eastern shore of Lake Michigan is particularly vulnerable to coastal erosion owing to the underlying geologic composition (G. Larson & Schaetzl, 2001; Norton et al., 2011) and long fetch distances parallel to the dominant west-to-east tracks of regional midlatitude cyclones which generate intense storm waves (Huang et al., 2021; Meadows et al., 1997). To develop the capacity to predict future beach erosion and accretion, it is necessary to understand the roles that fluctuations in hydrodynamics, particularly mean lake level and seasonal oscillations in wave energy, and the underlying morphological structure of the coastal profile play in sediment transport.

Background

Great Lakes Hydrodynamics

Unlike oceanic coasts, Great Lakes coastlines are subject to a much wider range of mean water levels instead of the steady, incremental rise of global mean sea level observed over the last century (Abdelhady & Troy, 2023; Hands, 1984). While the Great Lakes are large enough to be influenced by diurnal tidal cycles, they are often called North America's "tideless coast" because of the negligible magnitude of tidal fluctuations which range from 0.01 – 0.05 m (Hamblin, 1987; Quinn, 2002; Trebitz, 2006; Weishar & Wood, 1983). In addition to small tidal

fluctuations, hourly fluctuations in water level are primarily driven by seiches and range between 0.05 – 0.30 m (Trebitz, 2006; Wilcox, 2004). Lake levels also fluctuate seasonally between 0.20 – 0.40 m with the seasonal high water peak occurring during the summer due to high runoff throughout the spring and summer months and the lowest seasonal lake level occurring during the winter due to higher rates of over-lake evaporation in the fall and winter months (Lenters, 2001; Quinn, 2002; Thompson & Baedke, 1995). Over longer timescales, work analyzing the sediments contained in strand plane topography in beach ridges surrounding Lake Michigan found evidence for several temporal cycles of oscillations in lake level varying in magnitude from 0.50 – 0.60 m every 25 to 35 years, 0.50 – 1.50 m every 120 to 180 years, and 1.80 – 3.70 m every 500 to 600 years (Thompson, 1992; Thompson & Baedke, 1997). These longer-term fluxes in mean lake level are driven by variations in three climatic variables: over-lake precipitation, lake evaporation, and basin runoff (Deacu et al., 2012; Gronewold et al., 2016; Gronewold & Rood, 2019).

Within the last forty years, Lake Michigan water levels have exhibited an incredible amount of variability (Figure 1). Between 1982 and 1986 water levels rose to then record-setting high levels before returning to near average levels followed by a brief period of moderately elevated lake levels between 1994 and 1998. Between 1999 and 2013, Lake Michigan experienced an unusual, prolonged stand of low lake levels well below average values. Beginning in 2013, lake levels rapidly increased to a record-setting high in 2020 before beginning to fall again in 2021.

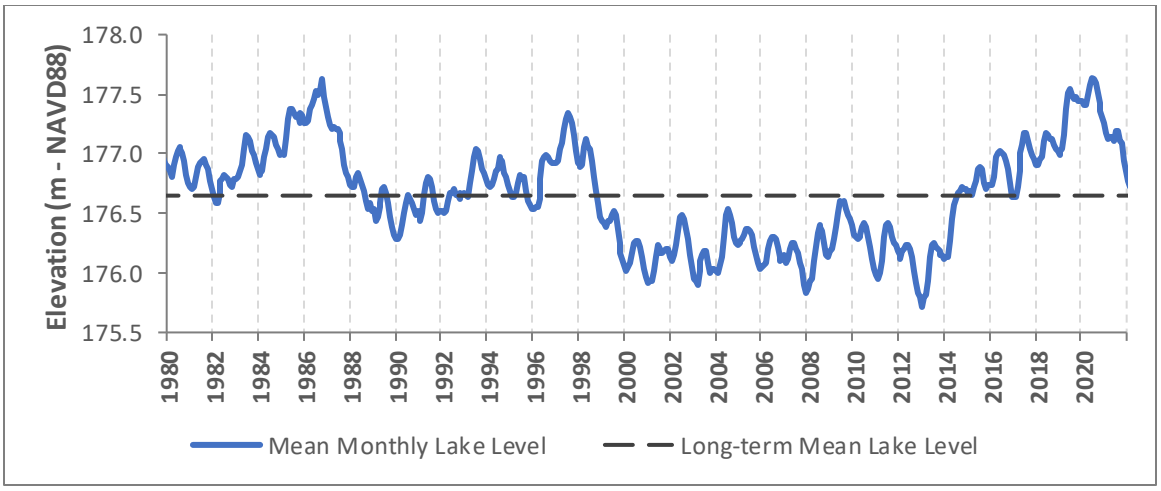

Figure 1. *Lake Michigan monthly mean lake level elevations from 1980 – 2021.* Elevations are reported in NAVD88. Data taken from NOAA gauges 9087031 (Holland, MI) and 9087023 (Ludington, MI).

Water levels in the Great Lakes are notoriously difficult to forecast due to the complexity of climatic variables which influence net basin supply (Deacu et al., 2012; Gronewold et al., 2016; International Joint Commission, 2012). However, accurate forecasts are invaluable because lake level fluctuations have both major ecological and socioeconomic impacts. Fluctuating water levels in the Great Lakes change shoreline ecosystems form and function (Evtimova & Donohue, 2016). For example, annual to decadal lake level fluctuations control the inundation, areal extent, and plant succession of critical Great Lakes coastal wetland habitat (Anderson et al., 2023; Keddy & Reznicek, 1986; Trebitz, 2006; Wilcox, 2004). Lake level variability also impacts navigation, hydropower production, municipal water supplies, and coastal recreation opportunities (Gronewold et al., 2013; Lino Grima, 1993; M. R. Phillips & Jones, 2006; Quinn, 2002). The impacts of water levels on coastal ecology and socioeconomic activities are important, but the most important geomorphic role of lake levels is modulating the zone of interaction between incident wave energy and the beach and nearshore profile. For the purposes of this study, this area of interaction is called the "active zone."

Like water levels, waves in the Great Lakes also exhibit seasonal fluctuation. Average wave heights increase due to stormy midlatitude cyclone activity in the fall and winter and decrease during more quiescent summer periods. Elevated wave energy during stormier periods generally results in beach erosion and offshore transport while calmer wave conditions tend to lead to beach accretion and onshore transport. One of the key functions of variations in wave energy, which are further adjusted by lake level, are changes to the dimensions of the active zone of the profile above the depth of closure (*DOC*) (Birkemeier, 1985; Hallermeier, 1978, 1981) and beneath the limit of wave runup (often denoted as R_2) (Gomes da Silva et al., 2020; Stockdon et al., 2006). It is important to note that the *DOC* and R_2 values do not represent absolute limits to sediment transport. Rather they serve as a best estimate of the extent of the most variable morphodynamic activity in the littoral zone (Brutsché et al., 2016; Gorman et al., 1998; Nicholls et al., 1999; Stive et al., 1993).

On Lake Michigan, lake levels and significant wave height (H_s), defined as the average of the highest third of observed wave heights, have a direct relationship where increases in mean H_s are coincident with periods of rising water levels (Huang et al., 2021). This relationship is potentially related to changes in storm frequency and intensity which in turn are likely tied to long-term regional climate variability (Huang et al., 2021; Meadows et al., 1997). With lake levels expected to become more variable in the future due to climate change (Gronewold & Rood, 2019) and an anticipated increase in over-lake precipitation and basin runoff projected to lead to an increase in Lake Michigan water levels of 0.44 m (with an uncertainty range of -0.13 to +0.80 m) by 2040-2049 (Kayastha et al., 2022), it is critically important to advance the quantitative understanding of relationships between hydrodynamic variables and long-term trends in erosion and accretion.

Great Lakes Morphology and Sediment Transport

Wave energy impacts facilitated by water levels are the primary driver of erosion and accretion, and hence of sediment transport. However, antecedent profile morphology, especially the profile slope and the cross-shore position of nearshore bars (Houser & Greenwood, 2005a, 2005b), combined with local wave climate are an integral part of determining the morphological state of the beach (Wright et al., 1985; Wright & Short, 1984) and facilitating LS and CS sediment transport.

The beach and nearshore profile morphology of the eastern shore of Lake Michigan has been a topic of great interest to researchers over the past eighty years. Multiple studies (e.g. Birkemeier, 1981; Davis, 1976; Davis & Fox, 1972; Evans, 1939, 1940; Hands, 1976, 1980, 1984; Saylor & Hands, 1970; Theuerkauf et al., 2022; Weishar & Wood, 1983; Wood & Weishar, 1984) have reported on the coastal geomorphology of the eastern coast of Lake Michigan and describe the typical profile structure found along unconsolidated sandy shorelines. The typical coastal profile structure of the beach and nearshore can be roughly divided into four sectors which each exhibit unique patterns of morphological change and are dominated by different coastal processes. These four sectors are the subaerial beach (sector A), the inner nearshore swash bar (sector B), the inner surf zone and nearshore bars (sector C), and the outer surf zone (sector D). Figure 2 diagrams each of these sectors and describes important morphological features and coastal processes associated with each sector. Previous studies have demonstrated the utility of classifying similar profile sectors based on vertical profile variations over time to better understand geomorphic change and to assess the role of LS and CS sediment transport processes in those changes (Almeida et al., 2011; López-Dóriga & Ferreira, 2017).

a) Beach and inner nearshore profile morphology (sectors A-B)

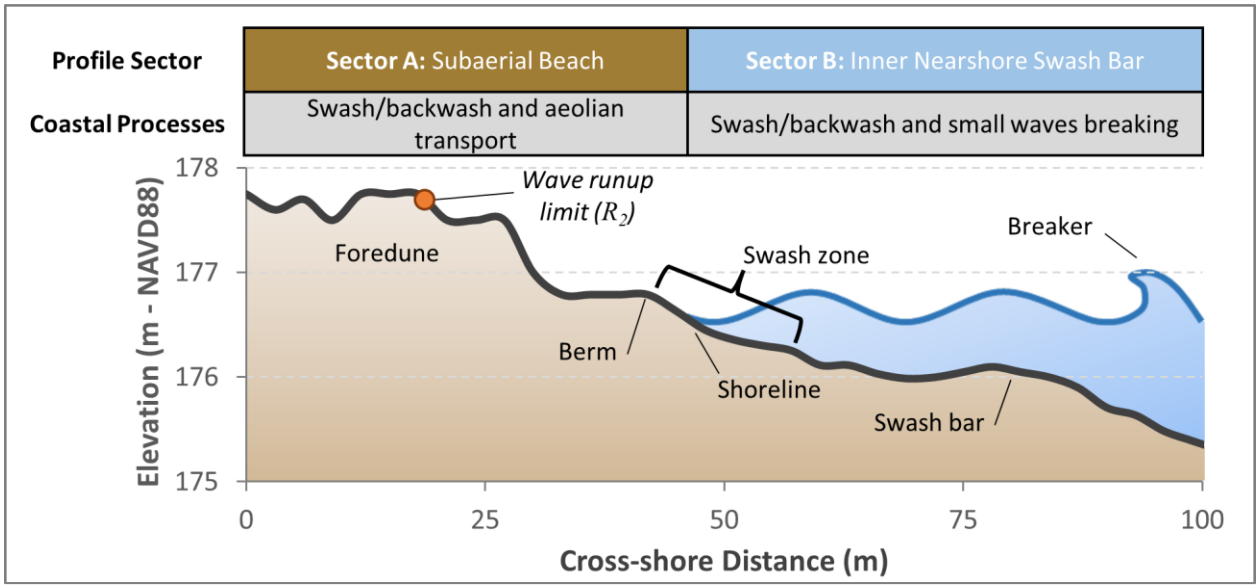

b) Coastal profile morphology (sectors A-D)

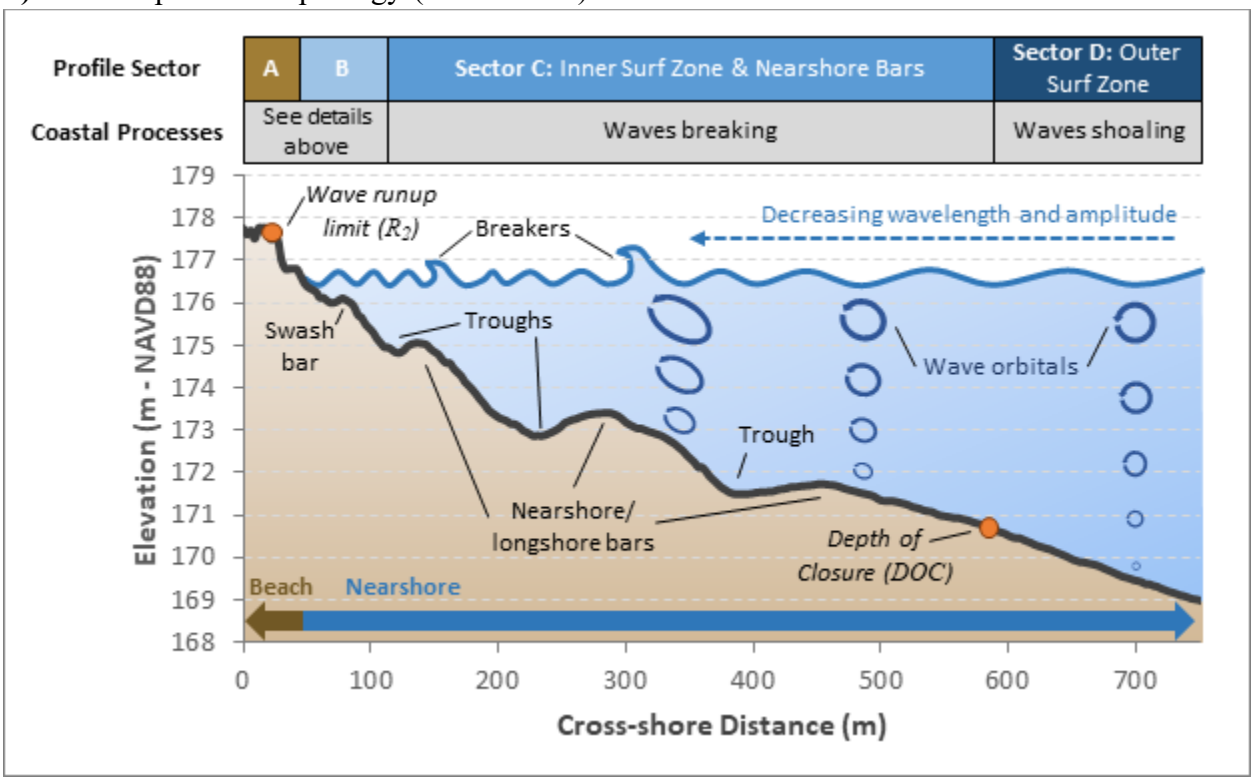

Figure 2. *Diagram of coastal profile morphology sectors and processes*. Figures display the characteristic profile morphology, sectors, and coastal processes of sandy beach coastal profiles in the Great Lakes. a) Shows a close-up of the morphology of sectors A and B (beach and inner nearshore swash bar). b) Displays an example of the coastal profile extent (sectors A-D) analyzed in this study and illustrates how waves interact with the lakebed as they shoal and break. Figure b) also illustrates where the average idealized locations of the boundaries of the littoral/active zone (wave runup (R_2) and depth of closure (DOC)) might typically fall.

Each section of the profile has different morphological and sediment transport characteristics. Sector A, which contains the subaerial beach, is the most visible zone of the profile structure, and its condition is usually what draws the most attention from the public and coastal managers alike (Hands, 1980). Sector A extends from the shoreline landwards towards the backshore (Figure 2a). Characteristic features of a subaerial beach on eastern Lake Michigan are a relatively flat-sloped beach backed by a foredune, bluff, or dune field. Sediment transport on beaches is closely associated with wave runup and is driven though the swash and backwash of waves. Sediments transported onshore via swash of incoming waves can then be mobilized by aeolian processes and blown into the backshore and contribute to foredune and dune growth. During storms, elevated wave energy levels can erode large amounts of geologic material from the beach or the backing foredune and deposit the eroded sediment offshore. In periods of high lake levels, larger storm waves can reach farther up along the profile and erode sediments which are relatively inaccessible to wave action during periods of low lake levels.

Moving lakeward from the beach, sector B contains the inner nearshore swash bar which is a shallow submerged feature of the profile which extends from the shoreline lakeward towards the inner surf zone and nearshore bars in sector C (Figure 2a). Sediment transport in this sector is dominated by swash zone processes as energy from breaking waves is dissipated across the profile in swash and backwash. The swash zone is an extremely active section of the profile which typically has the greatest concentration of suspended sediment of anywhere along the profile and serves an essential role as the conveyor belt for littoral drift (Butt & Russell, 2000; Elfrink & Baldock, 2002; Evans, 1939, 1940). The profile lakeward of the swash zone often develops a step-like feature which Evans (1939) initially described as a "nearshore terrace." This step serves as the base for a highly mobile sediment ridge which behaves similarly to swash bars

documented on marine coasts (Davis et al., 1972; Houser & Greenwood, 2007; M. S. Phillips et al., 2017). Due to the negligible influence of tidal water level fluctuations in the Great Lakes, the swash zone on Great Lakes coasts tends to be narrower than on marine coasts. This is one reason why the shallow swash bar on Great Lakes profiles can be mistaken as the first member of the nearshore bar system (Evans, 1939, 1940). However, because of how shallow this bar is, it is much more mobile than larger bars found farther offshore and lacks a consistent seasonal pattern of morphodynamic development (Weishar & Wood, 1983). As was noted earlier, this profile section is an important source of sediment for beach recovery during a quiescent post-storm period as small waves which lap over the crest of the swash bar produce onshore-directed transport and weld the swash bar to the shoreline (Davis, 1976; Houser, 2009; Morton et al., 1994).

Sector C encompasses the inner surf zone which contains a series of nearshore sandbars which store large amounts of unconsolidated sediment (Figure 2b). The nearshore bars of eastern Lake Michigan have generated an immense amount of scholarly inquiry and are occasionally also referred to as longshore bars. These sandbars are remarkable for their continuity along hundreds of miles of coastline (Evans, 1940) and are more permanent and well-developed features unlike the tidal bars found on marine coasts (Davis et al., 1972; Hands, 1984). This area's hydrodynamics are dominated by surf zone processes initiated by breaking waves. As waves approach the shore, the wavelength and amplitude of the wave decrease due to shoaling as wave orbitals encounter friction along the lakebed. This friction causes the wave orbitals to become more skewed and oversteepened until the waves eventually break. Within a multi-barred profile during periods of elevated wave energy, lines of wave breakers may form at the location

of each of the nearshore bars which act to dissipate incident wave energy and protect the beach from storm damage.

The location of the nearshore bars shifts in response to variability in hydrodynamic conditions. Over shorter timescales of hours to weeks, bar location is controlled by wave conditions. Dyhr-Nielsen & Sørensen's (1970) widely accepted breakpoint hypothesis of nearshore bar formation states that bars form and are maintained around an equilibrium point at the convergence of offshore-directed suspended sediment transport from the undertow of broken waves and onshore-directed bedload sediment transport from the lower shoreface. During periods of non-breaking, low-energy wave conditions, typically associated with spring and summer wave conditions in the Great Lakes, nearshore bars tend to migrate onshore while during periods of breaking, high-energy wave conditions, associated with late fall and winter wave conditions in the Great Lakes, nearshore bars tend to migrate offshore (Fox & Davis, 1973; Gallagher et al., 1998; Grossmann, Hurther, Sánchez-Arcilla, et al., 2023; Ruessink et al., 1999; Sallenger et al., 1985; Weishar & Wood, 1983). These shorter-term migrations in nearshore bar location along the profile appear to be closely associated with water depth above the bar crest and result in the movement of the bar crest toward the breakpoint location for a given wave condition (Eichentopf et al., 2020; Pape et al., 2010; Plant et al., 1999, 2001).

Over longer, interannual timescales, nearshore bars in the Great Lakes exhibit a lagged response to lake level fluctuations and typically shift shoreward and gain volume following an increase in lake level and move offshore and lose volume following a drop in lake levels (Hands, 1976, 1980; Saylor & Hands, 1970). Owing to the limited spatial resolution of previous studies, the nature of the lagged repositioning of nearshore bars following changes in lake level has not been quantitatively determined, with previous research speculating that the response often occurs

over a period of several years following a shift in lake levels (Hands, 1976, 1980; Wood et al., 1994). Due to the large fluctuations in nearshore bar location and crest depth beneath the water level, some researchers have speculated that during periods of prolonged low lake levels nearshore bars in the Great Lakes may be an important source of sediment for beach recovery and dune development (Bajorunas & Duane, 1967; Houser, 2009; Olson, 1958). However, the long-term degree of sediment connectivity between nearshore bars and the subaerial beach is still not well understood.

The final profile sector considered in this study, sector D, contains the outer surf zone (Figure 2b). Compared to the morphological features of the other three sectors of the coastal profile, this sector is rather simple and is characterized by a gentle slope from the lakeward edge of the outermost nearshore bar down towards the lake basin. This sector is the least active in terms of sediment transport. The limited amount of sediment transport which occurs in this sector is most likely limited to small amounts of onshore bedload transport initiated by shoaling waves and offshore-directed suspended transport during the most energetic storm conditions. It is important to note that the depth of closure for these extreme storm conditions typically occurs lakeward of this sector, and as a result a single strong storm event has the potential to suspend and transport unconsolidated material in this sector.

Research Questions

Although the knowledge of coastal profile morphology and the typical patterns of sediment transport across and along this morphology in the Great Lakes has been studied, a fundamental gap in the quantitative understanding of multidecadal sediment connectivity across these profiles remains. As a result, the ability to sustainably manage these coastlines with the

goals of mitigating the impacts of erosion and promoting beach recovery is limited. To begin to address this gap, two primary research questions were pursued by this study:

1) What is the degree of long-term sediment connectivity across the coastal profiles of sandy beaches in the Great Lakes?
2) How do long-term patterns of sediment exchange across the coastal profile contribute to the likelihood of beach recovery following periods of accelerated erosion during high lake levels?

To investigate these questions, this study utilized a unique multidecadal dataset of profile morphology surveys at six study sites along the eastern coast of Lake Michigan and a novel combination of methodologies based on established principles of hydrodynamics and sediment transport to analyze shifts in the active sediment transport zone during different morphodynamic conditions (MCs) described by different wave parameters. Specifically, this study analyzed three key elements of profile morphology and sediment transport:

1) how profile morphology changed over several decades,
2) the relative role and importance of LS and CS sediment transport in shaping profile morphology, and
3) where, when, and how different MCs interact with profile morphology and transport sediment.

This study is an initial investigation of broad-scale trends in interactions between accretionary and erosive wave conditions and various morphological configurations over multiple periods of rising and falling lake levels. As a result, this study aims to be an important first step towards quantitatively assessing the likelihood and rate of future beach recovery.

Study Area and Methods

Study Sites

From 1988 to 2000, a team of researchers at the Ocean Engineering Laboratory at the University of Michigan conducted periodic surveys of the beach and nearshore profile at sandy beaches along the eastern coast of Lake Michigan (Norton et al., 2011). A subset of six of these sites that were resurveyed by the Coastal Processes and Geomorphology Laboratory at Michigan State University in 2021 were selected as the study areas for this project. One of these sites (UM04) is located near New Buffalo, MI, one site (UM14) is in P.J. Hoffmaster State Park, MI, three sites (UM19, UM21, and UM22) are located around Ludington, MI, and the final site is located 2.5 miles north of Manistee, MI (Figure 3, Table 1). Four of these sites, UM04, UM19, UM21, and UM22, are all located in filets of harbor structures in sand-rich environments and were the locations for a recent study by Theuerkauf et al. (2022). UM14 and UM29 are not located near major harbor protection structures, but the beach at UM29 has been recently armored with riprap and is relatively narrow while the beach at UM14 is backed by large, vegetated dunes and is free of any shoreline armoring. More detailed descriptions of each site are available in Table 1.

All six of these sites have nearshore bathymetry characterized by multiple, temporally persistent bars and were selected for the quality and length of the profile survey record at the site. They were also selected to achieve a wide spatial distribution of study sites to analyze long-term changes in profile morphology across an extensive area of the eastern coastline of Lake Michigan.

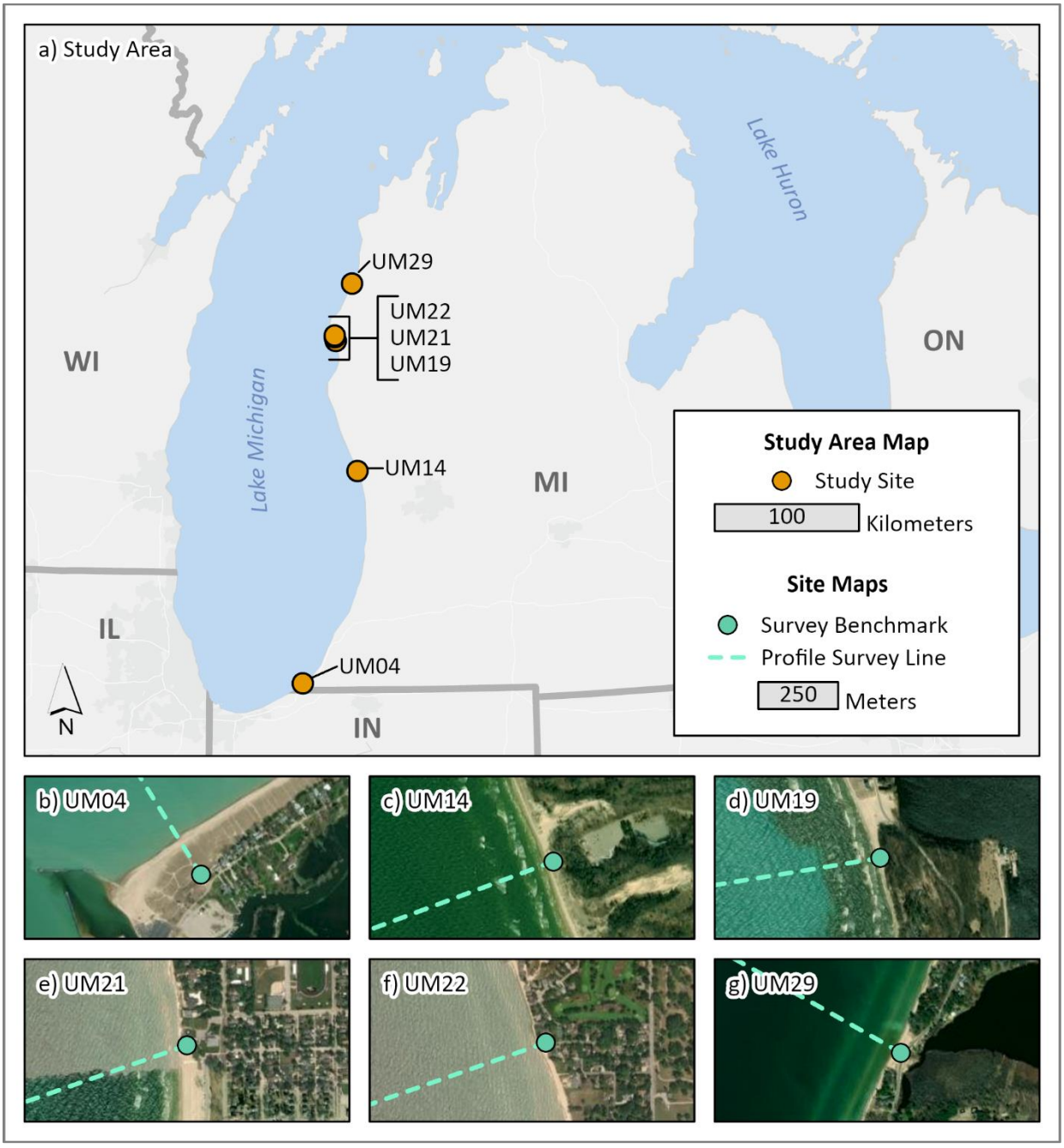

Figure 3. *Study area map.* a) Shows the general location of each study site along the eastern Lake Michigan coastline. b) – g) Site maps display large-scale views of each study site.

Site ID	Site Name	Profile Bearing (°)	Site Description and Notes
UM04	City Waterfront Park, New Buffalo Harbor North	328	Sandy beach backed by large foredune. Located 0.2 km north of the New Buffalo harbor jetty.
UM14	P.J. Hoffmaster State Park	250	Sandy beach backed by large, vegetated dunes and dune blowouts. Limited coastal development due to location in a state park.
UM19	Buttersville Park, Ludington Harbor South	261	Sandy beach backed by small, vegetated dunes. 1.5 km south of Ludington harbor breakwater. Small groin field to the north of the site. Coastline south of site is heavily armored.
UM21	Stearns Park, Ludington Harbor North	251	Wide sandy beach backed by foredune. Immediately south of the Ludington Water Plant's drain into Lake Michigan. 0.6 km north of Ludington harbor breakwater. Coastline north of the site was armored with riprap and seawalls.
UM22	Juanita Street Public Easement, Ludington Harbor North	251	Sandy beach backed by foredune. 1.7 km north of Ludington harbor breakwater. Surrounding coastlines are armored. Very heavy armoring north of the site.
UM29	Bar Lake Access, Manistee	300	Narrow sandy beach north of Bar Lake's outflow to Lake Michigan. Beach has been heavily armored with riprap.

Table 1. *Study site descriptions*. Profile bearings were the survey headings used to collect each profile. Site descriptions provide a brief report of the beach and any major coastal infrastructure or armoring at the site or along the adjacent shoreline.

Data Collection

Profile Data

Members of the Ocean Engineering Laboratory at the University of Michigan surveyed beach and nearshore profiles periodically from 1988 to 2000. In total, six of these survey records from each study site were used in this study. These data were collected during the summer in August 1988, August 1989, July-August 1996, July-August 1997, June-July 1998, July-August 1999, and June-August 2000. Benchmarks for repeatable profile measurements were established

at the top of local dunes or bluffs in 1988. Profiles were surveyed from these benchmarks out to an offshore depth of approximately 10 m along a bearing perpendicular to the orientation of the shoreline. Due to extensive shoreline erosion at some of these sites during the study period it was unsafe or impractical to start the survey from the established benchmark and the surveys were instead started from as close to the original benchmark as possible. Elevation and CS distance data for the subaerial beach and upper nearshore portions of the profile out to wading depth were surveyed using an engineer's automatic level. The elevation of the still water level relative to the benchmark was recorded at the time of each onshore survey. Bathymetric data for the remaining section of the nearshore profiles were collected using a single beam echosounder with survey overlap between the sonar and the wading survey data to allow for calibration of the bathymetry data. All survey data were adjusted to the water level at the time of the survey and referenced to the International Great Lakes Datum of 1985 (IGLD85) low water datum for Lake Michigan. The overall vertical and horizontal accuracies of these data were not calculated at the time of the survey. However, similar survey techniques using an engineer's automatic level to collect profile data at coastal sites along Lake Michigan in the 1960s and 70s reported overall vertical profile accuracies of ± 0.05 m (Hands, 1979).

The survey lines at these sites were resurveyed by researchers at Michigan State University in August-September 2021 using updated survey equipment technology. Topographic data for the subaerial beach and bathymetry data for the upper nearshore out to wading depth were collected using a Trimble R10-2 Real-time Kinematic Global Positioning System (RTK-GPS). Horizontal and vertical accuracies for these data range from 0.01 – 0.02 m. Bathymetry data for the rest of the nearshore portion of the profile were collected using the RTK-GPS system in conjunction with a SonarMite 200 kHz single beam echosounder. Due to the draft of the

research vessel used for bathymetric surveying, the vessel could not get close enough to shore to overlap with the observations surveyed out to wading depth. Horizontal and vertical accuracies for these data range from 0.05 – 0.10 m. Horizontal position data collected during the topographic and bathymetric surveys were referenced to NAD 1983 UTM Zone 16N and elevation data were vertically referenced to the North American Vertical Datum of 1988 (NAVD88).

Topobathy LiDAR data collected in 2008 and 2012 by the U.S. Army Corps of Engineer's (USACE) National Coastal Mapping Program (NCMP) was accessed from the National Oceanic and Atmospheric Administration's (NOAA) Data Access Viewer to fill in the gap between the 2000 and 2021 field surveys (Joint Airborne Lidar Bathymetry Technical Center of eXpertise (JALBTCX), 2022a, 2022b). These LiDAR data were downloaded in raster format with 3 m cell resolution with the horizontal datum set to NAD 1983 UTM Zone 16N and the vertical datum set to NAVD88. The 2008 data had a vertical accuracy of 0.20 m and a horizontal accuracy of 0.75 m and were collected from 7/28/2008 – 9/16/2008. The 2012 data had a vertical accuracy of 0.15 m and a horizontal accuracy of 0.50 m and were collected from 9/02/2012 – 10/19/2012 and 11/05/2013 – 11/26/2013. Combining all three collection types of profile surveys together, each study site had a total of nine survey periods: 1988-1989, 1989-1996, 1996-1997, 1997-1998, 1998-1999, 1999-2000, 2000-2008, 2008-2012, and 2012-2021.

Hydrodynamic Data

Hourly records for significant wave height (H_s), wave peak spectral period (T_p), and wave mean direction (θ) downloaded from the U.S. Army Corps of Engineers Wave Information Study (WIS) wave hindcast model database (U.S. Army Corps of Engineers, 2023) were used as the wave descriptors for this study. WIS data were downloaded from 1/1/1988 – 12/31/2021 from the

nearest WIS station with the most complete record at each study site. These data were used as the primary wave data for each study site. Data from surrounding WIS stations were also downloaded and used to fill data coverage gaps at the primary WIS station. Additional information about the WIS stations used in this study can be found in Appendix A.

Hourly records for Lake Michigan water levels between 1/1/1988 – 12/31/2021 were downloaded from NOAA's National Ocean Service (NOS) tide gauges 9087031 (Holland, MI) (National Oceanic and Atmospheric Administration, National Ocean Service, Center for Operational Oceanographic Products and Services, 2023b) and 9087023 (Ludington, MI) (National Oceanic and Atmospheric Administration, National Ocean Service, Center for Operational Oceanographic Products and Services, 2023a) with water level elevations referenced to the IGLD85 vertical datum. Water levels from the Holland, MI, gauge were used for UM04 and UM14 while the water level data from the Ludington, MI, gauge were used for UM19, UM21, UM22, and UM29.

Data Processing

Profile Data Processing

Prior to data analysis, some additional data processing and cleaning of the profile data was necessary to facilitate comparison of profile elevations throughout the timeseries. The initial profile data processing and analysis was performed using Microsoft® Excel® (Microsoft, 2023) software unless otherwise noted. The elevation data for profiles collected between 1988 and 2000 were converted from IGLD85 to NAVD88 using conversion factors provided by NOAA's National Geodetic Survey's IGLD 85 Height Conversion tool (National Oceanic and Atmospheric Administration, National Geodetic Survey, 2018). Bathymetric data generated

during the 2021 surveys contained some noisy data artifacts due to the survey vessel motion, and these points were visually inspected and removed manually.

Due to wave conditions or the need to deviate from the survey line to avoid obstructions in the water, some of the 2021 survey data were not collected directly along the historically established survey lines and were horizontally displaced by an average of 8.9 m across all study sites. To account for the slight differences in survey headings and align CS distances of the different surveys, these observations were snapped to the historical survey line using the Snap tool in ESRI's ArcGIS Pro software (Environmental Systems Research Institute, 2021).

Following these steps, all profile data were brought into ESRI's ArcGIS Pro software (Environmental Systems Research Institute, 2021) for additional processing. Small holes in the 2008 and 2012 LiDAR data were interpolated using the Focal Statistics tool. To match the 3 m spatial resolution of the 2008 and 2012 profiles, the profiles surveyed in the field were interpolated using the Spline with Barriers tool. This tool was selected after testing several interpolation methods because it generated the most natural-looking outputs through its minimum curvature surface gridding technique which compared the weighted sum of 12 neighboring cells to interpolate new values. To measure the uncertainty in the interpolated profile results, 10% of survey observations were withheld for an accuracy assessment. These points were selected randomly from a subset of non-sequential soundings from the bathymetry data at each site and excluded any topographic observations because many surveys had very limited numbers of surveyed points on the subaerial beach.

Due to field conditions at the time of the surveys, not all profiles started at the survey benchmark or terminated at the same distance offshore from the benchmark. To enable comparison throughout the timeseries, profiles were clipped both onshore and offshore to the

maximum shared common profile extent between all surveys. An example of what the unclipped and clipped profiles looked like at UM14 is provided in Appendix B. Finally, for each profile survey line, a series of points spaced at 3 m were generated from the common starting point out to the common ending point. The predicted values of the interpolated profiles and the values of the LiDAR rasters which intersected with each point were extracted and used as the profile elevation data in subsequent analysis.

Hydrodynamic Data Processing

Hourly lake level elevation data were converted from IGLD85 to NAVD88 using conversion factors provided by NOAA's National Geodetic Survey's IGLD 85 Height Conversion tool (National Oceanic and Atmospheric Administration, National Geodetic Survey, 2018). Any gaps in the records of either the Holland or Ludington gauges were filled in where possible with data from the other gauge. In total, only 0.016% of records were missing from the lake level data. Missing records from the primary WIS station at each site were filled where possible using the average of the data from nearby stations. The number of stations used to create this average varied from site to site depending on the density of WIS stations in the area and the number of those adjacent stations which also had concurrent gaps in their own records. Overall, the total percentage of coverage gaps was 3.28% at UM04, 2.79% at UM14, 1.95% at UM19, UM21, and UM22, and 1.68% at UM29. (See Appendix A for additional information.)

Data Analysis

Profile Sector Classification and Areal Change

The first step in analyzing the profile data was to classify morphodynamically unique sectors of each profile. Following Almeida et al.'s (2011) method, the profile was subdivided at nodes (points of lower variability) which were separated by one or more antinodes (points of

higher variability) on the plot of the standard deviation of all profile surveys at each site. Figure 4 shows an example of how sectors were classified using this method at UM04 and UM14. (Similar graphs for all study sites are available in Appendix C.)

Most profiles were divided into the four major sectors described in the introduction. The boundary between sectors A and B was placed at the node closest to the average CS position of the shoreline throughout the study period. The boundary between sectors B and C was placed at the node closest to the farthest shoreward location of a clearly visually discernable nearshore bar during the study period. Finally, the boundary between sectors C and D was placed at the node closest to where the standard deviation of profile elevations fell and remained below 0.3 m. This cutoff was chosen because changes of this magnitude were well within the margin of error of the vertical accuracies for the profile data used in this study. UM21 only had sectors A-C, but all other sites had all four profile sections. To measure smaller-scale shifts in sediment within the four major sectors, subsector boundaries were placed at smaller nodes within the major sectors. As a result, some major sectors were split into two or more subsectors. The number of subsectors identified varied widely across study sites. (See Appendix C for more information.)

a) UM04

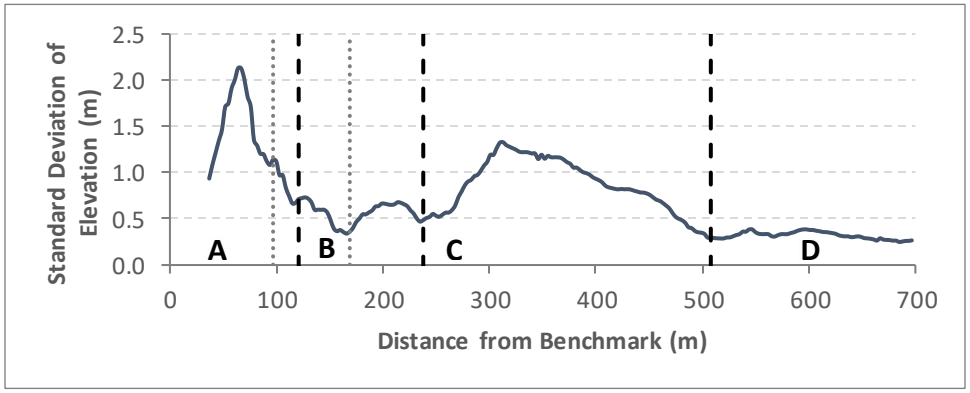

b) UM14

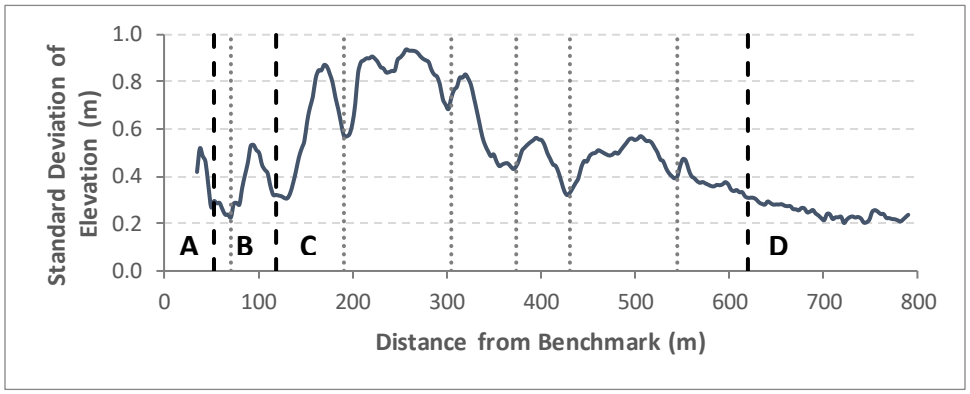

Sector Boundary Subsector Boundary

Figure 4. *Examples of classification of cross-shore profile sectors at UM04 and UM14 based on standard deviations of profile elevations.* Sector boundaries are shown at nodes between profile sections. Subsector boundaries are placed at smaller nodes which occur within major sectors before a transition to a different sector type.

To quantify long-term trends in the geomorphic change of the profiles, the area under the profile curve was measured for each survey by subsector. Figure 5 shows an example of the morphological change between two profile surveys at UM14 and identifies the part of the area under the profile that was measured. Areas were calculated using a simple rectangular estimation approach where the minimum recorded elevation observed throughout the entire study period at each site (the baseline identified in Figure 5) was subtracted from the elevation of each profile observation. That difference was then multiplied by the distance between profile observations, which was typically 3 m, to measure the area of the rectangle between the surveyed minimum

and the profile elevation being considered. These area totals were summed for each profile sector and subsector and the difference in sector and subsector profile areas for each survey period and the net differences in sector and subsector profile areas were calculated.

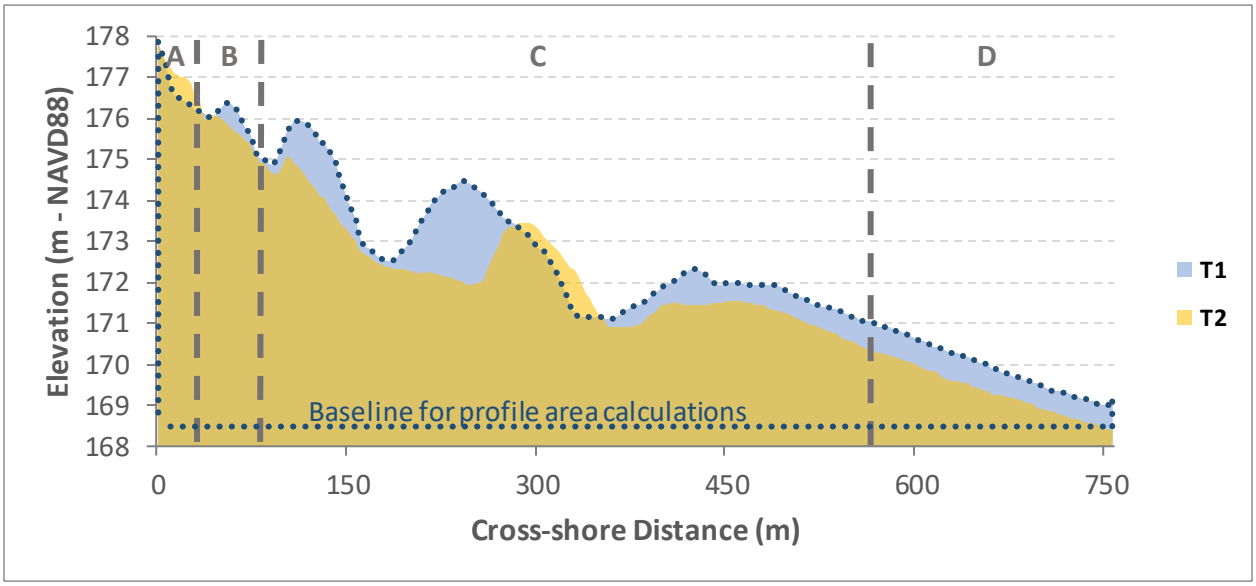

Figure 5. *Calculating change in profile area*. An example of the areal change in coastal profile morphology between T1 (1996) and T2 (1998) at UM14. The area which fell within the dashed outline around the area of T1 was summed up and recorded as the total profile area for that survey. These areal measurements were also taken for each sector and subsector. The bottom dashed line labeled as the baseline for profile area calculations is the minimum elevation value observed throughout the entire study period at this site (observed in 1998) and was used as the base elevation for calculating profile areas for each survey at this site.

LS and CS Sediment Transport

The changes in the profile area of subsectors at each study site were then used to quantitatively estimate the relative dominance of LS and CS sediment transport processes and connectivity for each survey timestep and across the entire study. This assessment was carried out using the LvC index created by López-Dóriga and Ferreira (2017) who used Almeida et al.'s (2011) profile sector classification method. The LvC index is a ratio which compares how much sediment was redistributed by CS sediment transport across the profile to how much sediment was gained or lost from the profile due to LS sediment transport during a given survey period.

The index is based on the observation that if the loss of sediment from one profile subsector is made up for by a corresponding gain of sediment in another profile subsector, CS processes are likely more prevalent. However, if the gains of sediment in one subsector cannot be accounted for by simultaneous losses of sediment from other subsectors or vice versa, LS processes are likely more prevalent. The LvC index ranges between -1 and 1 and is given by a modified version of Equation 2 in López-Dóriga and Ferreira (2017):

$$-1 \leq \sum_{i=0}^{n} \Delta A_i \Big/ \sum_{i=0}^{n} |\Delta A_i| \leq 1 \qquad (1)$$

where ΔA_i represent the change in profile area between surveys for each profile subsector. Figure 6 provides a visual illustration of the range and meaning of LvC index values. Positive LvC index values indicate profile accretion, while negative LvC index values indicate profile erosion. An LvC index value between -0.5 and 0.5 reflects the relative dominance of CS sediment transport, while values less than -0.5 or greater than 0.5 represent the relative dominance of LS sediment transport. The LvC index was calculated using changes in profile area observed in each study period and for the net change in profile area observed between the 1988 and 2021 profiles at all study sites.

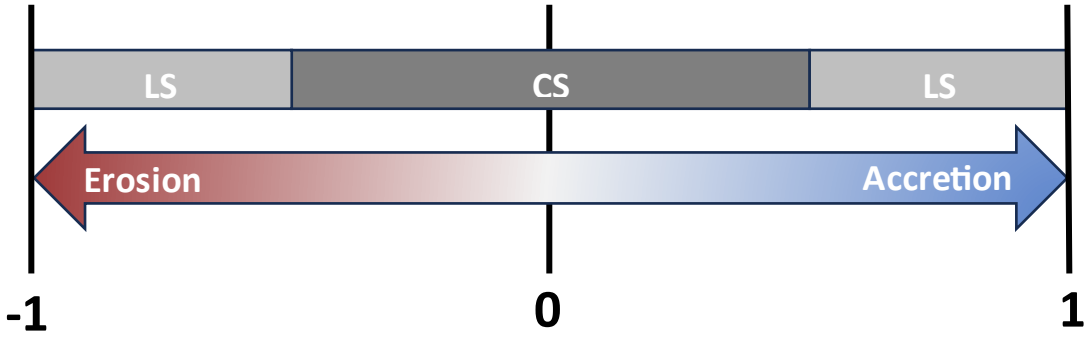

Figure 6. *LvC index*. Illustration of the range of values for the LvC index and the associated interpretations. Positive values indicate profile accretion, and negative values indicate profile erosion. LvC values between -0.5 and 0.5 indicate the dominance of CS processes, while values less than -0.5 and greater than 0.5 indicate the dominance of LS processes.

All subsequent analyses were coded and performed using R Statistical Software (v4.1.2) (R Core Team, 2023) unless otherwise noted. Functions from the readxl (Wickham & Bryan, 2023) and openxlsx (Schauberger & Walker, 2023) R packages were used to import and export spreadsheet data from Microsoft® Excel®. Specialized functions from the dplyr (Wickham et al., 2021), tidyr (Wickham, 2021), and plyr (Wickham, 2011) R packages were also used to analyze the data.

To further establish long-term trends in the role of LS and CS sediment transport at each site, the average wave direction, wave incidence angle, and LS and CS velocity vectors for each MC were calculated for each study site across the entire study period using an average of vectors method. Calculating the average wave direction through vector analysis was more accurate and meaningful than simply taking the average of the mean wave direction variable provided by the WIS data because of the difficulties associated with averaging data collected in circular coordinate systems. The average wave direction was calculated using:

$$\theta_{wave} = \left[360 + \left(\left(\text{atan2}\left(wv_x, wv_y\right)\right)\left(\frac{180}{\pi}\right)\right)\right] \bmod 360 \tag{2}$$

where wv_x was the horizontal vector and wv_y was the vertical vector given by:

$$wv_x = \sum(v_w\,[\sin(\theta(180/\pi))])/n \tag{3}$$

$$wv_y = \sum(v_w\,[\cos(\theta(180/\pi))])/n \tag{4}$$

where v_w is the velocity of the wave and n is the number of observations in the survey period. The horizontal (CS) and vertical (LS) vector components of the average wave vector were then calculated normalized to the shoreline for each MC at every study site.

Morphodynamic Condition Classifications

MC classifications were defined to determine the frequency of accretionary and erosive waves and where along the coastal profile these forces had the potential to suspend sediment and

rework profile morphology. Based on the work of Wright and Short (1984) which established a classification system for morphodynamic beach states based on dimensionless sediment fall velocity (Ω) (Dean, 1973; van der Meulen & Gourlay, 1968), laboratory experiments by Pape et al. (2010) and Grossmann et al. (2022) demonstrated that different values of dimensionless sediment fall velocity could be used to classify the direction of sediment transport under different wave conditions. In both Pape et al. (2010) and Grossmann et al. (2022), values of $\Omega < 2$ corresponded to onshore-directed sediment transport and beach accretion, while values of $\Omega \geq 2$ corresponded to offshore-directed sediment transport and beach erosion.

In this study, three MCs were classified: accretionary (AC), moderately erosive (ME), and severely erosive (SE). Erosive states were split into two categories using differences in significant wave height (H_s) to separate the impacts of high-frequency, lower-energy erosive conditions (ME) and low-frequency, high-energy stormy wave conditions (SE). The wave characteristics of AC conditions will tend to produce onshore-directed sediment transport while the wave characteristics of ME and SE conditions will tend to generate offshore-directed sediment transport. The MCs were defined using the following parameters:

$$\mathrm{MC} = \begin{cases} \mathrm{AC}, & \Omega < 2 \\ \mathrm{ME}, & \Omega \geq 2 \wedge H_s < 2 \text{ m} \\ \mathrm{SE}, & \Omega \geq 2 \wedge H_s \geq 2 \text{ m} \end{cases} \tag{5}$$

Dimensionless sediment fall velocity is given by:

$$\Omega = H_{rms}/T_p w \tag{6}$$

where H_{rms} is the root mean square wave height and w is the sediment fall velocity. H_{rms} was calculated using a formula created by the USACE Coastal Engineering Research Center (1984) given as:

$$H_{rms} = H_s/1.416 \tag{7}$$

Sediment fall velocity was calculated using Equation 4 from Ahrens (2000) and is given by:

$$w = C_l \Delta g d^2 / \nu + C_t \sqrt{(\Delta g d)} \quad (8)$$

where $\Delta = \rho_s - \rho / \rho$ (where ρ_s is the density of the sediment particle and ρ is the density of the fluid), g is the acceleration of gravity, d is the characteristic sediment particle diameter, ν (the lowercase Greek letter nu) is the kinematic viscosity of water, C_l is a coefficient associated with laminar flow, and C_t is a coefficient associated with turbulent flow. A value of 1.65 was used for Δ. This value is within the typical range used for sandy sediments and assumes the sediment is primarily composed of quartz and is being transported through freshwater (Bosboom & Stive, 2023). A value of 0.3035 mm was used as the value for d. This value was taken from Fingleton (1973) and is the mean of the range of mean sediment grain sizes of beach sediments collected at seventeen sandy beaches along the eastern coast of Lake Michigan between the Michigan/Indiana state line and Frankfort, MI. The value of ν for freshwater was calculated using a modified version of Equation 7 from Ahrens (2000) and is given by:

$$\nu = (c_0 + c_1 T + c_2 T) / 10^4 \quad (9)$$

where T is water temperature between 0 – 30°C, c_0 is 0.0178, c_1 is -0.000529, and c_2 is 0.0000069. The values of coefficients C_l and C_t were derived by Ahrens (2000) for quartz sediments and are given by:

$$C_l = 0.055 \tanh[12 A^{-0.59} \exp(-0.0004 A)] \quad (10)$$

$$C_t = 1.06 \tanh[0.016 A^{0.5} \exp(-120/A)] \quad (11)$$

where A is the Archimedes buoyancy index. The value of A is calculated as:

$$A = \Delta g d^3 / \nu^2 \quad (12)$$

Dimensionless sediment fall velocities were calculated for each hourly record in the WIS dataset for each site using a month-specific value of kinematic viscosity calculated using the

long-term monthly mean water temperature recorded at the Holland, MI, NOAA NOS gauge. These month-specific values of kinematic viscosity were calculated using Microsoft® Excel® (Microsoft, 2023) and were then brought over into R Statistical Software (R Core Team, 2023) Data for the monthly mean water temperature were accessed from the NOAA National Center for Environmental Information (NCEI) Coastal Water Temperature Guide (National Oceanic and Atmospheric Administration, National Ocean Service, 2023). This information was not available from the gauge at Ludington, so the data from Holland were used for all study sites.

Sediment Mobilization Likelihood

Having classified different MCs, the next step was to identify where along the profile sediment had the potential to be suspended and transported by each MC. To calculate the elevation of the *DOC* for each hourly record in the WIS data sets, Equation 3 from Hallermeier (1978) was modified to include a term for lake level and was calculated as

$$DOC = h - (2.28H_s - 68.5(H_s^2/gT_p^2)) \tag{13}$$

where *h* is the lake level elevation. The elevation of wave runup, defined as the height above lake level exceeded by the top 2% of wave runup peaks, was calculated using Equations 18 and 19 from Stockdon et al. (2006) modified to calculate height above lake level and is given by

$$R_2 = \begin{cases} h + 0.043\sqrt{(H_0L_0)}, & \xi_0 < 0.3 \\ h + 1.1(0.35\beta_f\sqrt{(H_0L_0)} + \sqrt{[H_0L_0(0.563\beta_f^2 + 0.004)]}/2), & \xi_0 \geq 0.3 \end{cases} \tag{14}$$

where H_0 is deepwater significant wave height, L_0 is deepwater wavelength, β_f is the foreshore beach slope in radians, and ξ_0 is the Iribarren number. The value of H_s was used as the value of H_0 since most WIS stations are located out beyond shoaling depth (For additional detail, see information on WIS station depth in Appendix A.), and L_0 was also calculated using H_s. In Stockdon et al.'s (2006) work, the calculation of β_f is not defined, although the foreshore is

typically defined as the intertidal zone of the profile (McGlashan et al., 2005). Because of the almost negligible tidal range in the Great Lakes, a different range was used to calculate slope for this study. Work by Gomes da Silva et al. (2020) suggests that a slope value which is calculated across the entire nearshore is preferable for R_2 calculations given the fact that shoaling and breaking waves interact with the slope of the entire nearshore profile above shoaling depth. For this study, the value for β_f was defined at each site as the average of the slopes of all surveyed profiles between the maximum offshore extent of the profile, which was within the maximum shoaling depth, and the upper limit of the swash zone (See Figure 2a). Following Gomes da Silva et al. (2020), the upper limit of the swash zone for each survey period was calculated as the elevation of mean lake level plus two standard deviations of the series of vertical oscillations about the mean lake level within each survey period. The Iribarren Number, also called the surf-similarity parameter, is a commonly used metric of dynamic beach steepness and was developed by Battjes (1974) based on the work of Iribarren and Nogales (1949) and is given by:

$$\xi_0 = \tan\beta / \sqrt{(H_0/L_0)} \tag{15}$$

where β is the beach slope in radians. The same value used for β_f in Equation 14 was used as the value for β in this study. Values of ξ_0 are often used to classify different wave breaker types and the dissipative vs. reflective behavior of any given beach. Values of $\xi_0 < 0.3$ reflect extremely dissipative conditions, and the value of R_2 can be reliably predicted with a less computationally expensive formulation (see Equation 14).

Using the above equations, the upper and lower limits of the active zone were calculated for each hourly record in the WIS data. Calculating DOC and R_2 in terms of elevation with respect to the hourly recorded lake level allowed this analysis to control for the effects of water level fluctuations throughout the study. Using the profile measured at the beginning of each

survey period, the total number of hours that each elevation along the profile and each major profile sector was within the active zone during each MC for that survey period was calculated. This was repeated for each survey period and the raw counts were normalized to show the likelihood of sediment mobility at each observation along the profile for every MC. The result was a series of data which showed the mean sediment mobilization likelihood for each MC at each observation along the profile. The mean sediment mobilization likelihood numbers were then totaled for each MC within each profile sector.

Profile Active Zone Summary Statistics

Finally, to better understand where the upper and lower limits of the active zone for each MC intersected with the morphology of each surveyed profile, the average DOC and R_2 values for the wave conditions associated with each MC were calculated for each study site. To understand the wave characteristics associated with the different active zone ranges for each MC at every study site, the average values for H_s and T_p were calculated. To quantify where the limits of the active zone fell during the most energetic wave conditions associated with each MC, the average of the DOC and R_2 values associated with the effective wave height (H_e) and the corresponding effective wave period (T_e) were calculated. The effective wave height is the wave height only exceeded for 12 hours out of a year, which is equivalent to the highest 0.137% of waves observed every year (Brutsché et al., 2016; Hallermeier, 1978; Nicholls et al., 1999) and was calculated as the 99.863 percentile of significant wave heights for each MC at each study site. The effective wave period is the average of the T_p values recorded when the H_s values exceed H_e. The average of the DOC and R_2 values associated with H_e values were called the effective DOC (DOC_e) and the effective R_2 ($R_{2,\,e}$). These mean DOC_e and $R_{2,\,e}$ limits for each MC for the entire study period were plotted on top of graphs of the 2021 profile morphology.

These graphs helped identify parts of the 2021 profile that fell within the active zone of each MC to assess the potential role different sectors might play in beach recovery following the most recent period of high lake levels.

Results

Profile Morphology Change

Profile Interpolation Accuracy Assessment

The results of the accuracy assessment conducted on the interpolated profiles are presented in Table 2. The total RMSE for the vertical accuracy assessment across all profiles and all surveys was 0.30 m. There is considerable variability in the individual RMSE values of each profile, with some exceptionally low values, such as 0.02 m at UM04 and UM22 for the 1999 data collection, and some higher RMSE values, such as 1.03 m at UM21 in 1996 and 1.02 m at UM14 in 1999. Overall, UM04, UM19, and UM22 had RMSEs at least half of those of UM14, UM21, and UM29. Combined with the vertical accuracies of the original data sources, the overall final vertical accuracy range for the profiles in this study was 0.15 – 0.54 m.

Site ID	Variable	1988	1989	1996	1997	1998	1999	2000	2021	Total
UM04	*RMSE (m)*	0.17	0.30	0.21	0.05	0.08	0.02	0.32	0.11	**0.15**
	n	8	7	7	14	13	14	4	24	91
UM14	*RMSE (m)*	0.23	0.15	0.11	0.16	0.04	1.02	0.07	0.04	**0.37**
	n	8	7	10	14	13	14	16	32	114
UM19	*RMSE (m)*	0.08	0.28	0.03	0.03	0.10	0.06	0.05	0.06	**0.08**
	n	11	5	10	13	12	10	15	34	110
UM21	*RMSE (m)*	0.09	0.23	1.03	0.12	0.03	0.03	0.02	0.80	**0.49**
	n	15	6	9	10	15	11	16	25	107
UM22	*RMSE (m)*	0.10	0.07	0.11	0.10	0.05	0.02	0.05	0.11	**0.09**
	n	14	9	7	14	13	11	16	29	113
UM29	*RMSE (m)*	0.05	0.18	0.08	0.21	0.04	0.04	0.84	0.03	**0.35**
	n	15	6	11	16	16	14	20	24	122
									Total RMSE (m)	**0.30**

Table 2. *Profile interpolation accuracy assessment results.* Displays the RMSE and number of points (*n*) used for the accuracy assessment of each interpolated profile at every study site.

Profile Areal Changes

The area of each profile sector and subsector was calculated to quantitatively assess geomorphic change over the study period. Table 3 summarizes these trends by sector and Figure 7 displays changes in profile areas by sector. Total profile areas changed relatively little over the entire study period. The net change in total profile area of all sites except UM04 was less than ±5.20%, but the net change in profile area at UM04 was 20.61%. Rates of interannual change in profile areas by subsector ranged between -1.90% and 16.80%, but the average rates of change for the majority of profile subsector areas between surveys ranged between -0.53% and 1.47%.

Throughout the study period, only UM04 and UM19 exhibited a net increase in profile area, while all other sites experienced a net decrease in profile area. At UM04, UM21, UM22, and UM29 sector A exhibited the greatest vertical variability and had the highest standard deviation value of all sectors. However, at UM14 sector C had the greatest variability and at UM19 sector B had the greatest variability. For most of these sites, the subaerial beach and the nearshore bars were the most dynamic and variable components of the profile.

Study Site	Change Parameter	Sector A	Sector B	Sector C	Sector D	Total Profile
UM04	Net (m^2/m)	3.09	1.16	0.82	-0.28	0.86
	Net Pct.	34.33%	18.81%	23.69%	-16.39%	20.61%
	S.D.	0.58	0.34	0.48	0.46	0.27
UM14	Net (m^2/m)	0.73	0.13	-0.28	-0.21	-0.20
	Net Pct.	9.13%	1.75%	-6.51%	-17.86%	-5.17%
	S.D.	0.46	0.34	0.18	0.18	0.16
UM19	Net (m^2/m)	-0.60	0.64	0.44	-0.17	0.08
	Net Pct.	-7.63%	10.29%	9.48%	-8.87%	2.11%
	S.D.	0.88	0.31	0.45	0.12	0.15
UM21	Net (m^2/m)	0.02	0.10	-0.07	--	-0.04
	Net Pct.	0.28%	1.80%	-2.03%	--	-0.90%
	S.D.	1.09	0.44	0.28	--	0.26
UM22	Net (m^2/m)	-0.82	-0.43	-0.02	-0.09	-0.12
	Net Pct.	-9.01%	-5.65%	-0.45%	-5.06%	-3.01%
	S.D.	0.89	0.25	0.51	0.18	0.28
UM29	Net (m^2/m)	0.41	0.45	-0.19	-0.30	-0.14
	Net Pct.	5.23%	6.69%	-4.95%	-26.72%	-3.64%
	S.D.	0.55	0.26	0.14	0.20	0.12

Table 3. *Summary of changes in coastal profile area, 1988 – 2021.* Displays the net change, net percentage change, and standard deviation (S.D.) of profile area changes by morphodynamic sector and across the entire profile for the study period (1988 – 2021). To enable cross-site comparison, net changes in area were normalized and are reported in m^2/m.

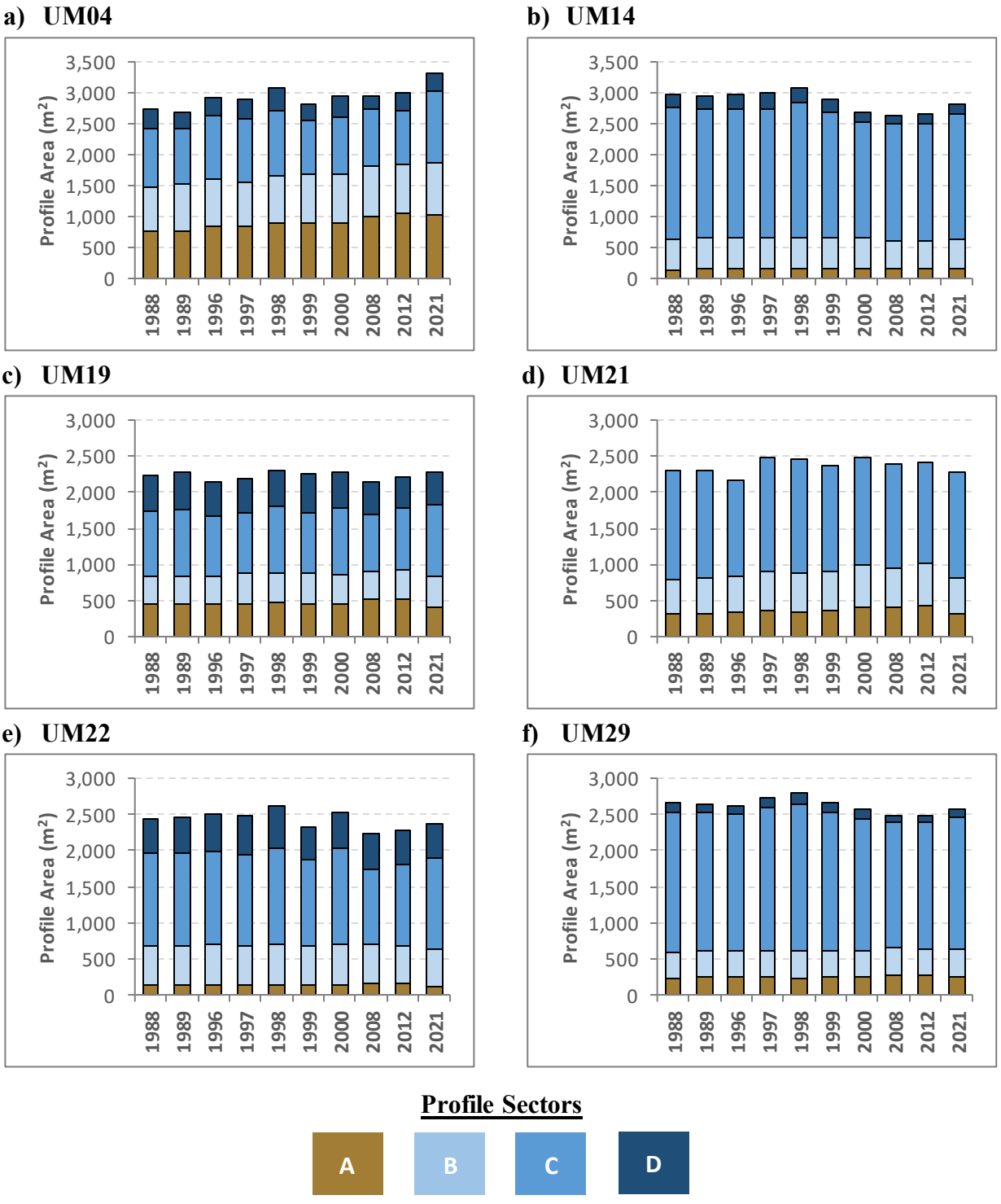

Figure 7. *Changes in beach and nearshore profile areas, 1988 – 2021.* Graphs display long-term variations in profile areas grouped by morphological sector for each profile survey.

While changes in sector profile area generally exhibit site-specific variability, the general trends in total profile area tend to correspond to lake level fluctuations during different survey periods. Between 1988 and 1996, lake levels decreased from the then record-setting high lake levels recorded in 1986 and stabilized around the long-term average lake level. Throughout this period, profile areas remained relatively stable at all sites, except for UM29, and experienced accretion in sector A. Subsequently, as lake levels rose again between 1996 and 1998, profile areas all increased until most, except for UM04, reached the maximum observed profile area of the entire study period in 1997 or 1998. This gain in sediment was primarily driven by an increase in the amount of sediment in the nearshore bars and the outer surf zone in sectors C and D while sector A tended to lose area. Following a smaller peak in lake level in 1998, most profiles lost area in 1999 but then gained some of the lost area back immediately in 2000 with the largest losses occurring in sectors C and D as sectors A and B tended to increase in area during this period.

Between 2000 and 2012 there was an unusually long period of below-average lake levels which marked a unique period of profile morphology change. During this period of low lake levels, profiles tended to lose area from 2000 to 2008 and then slightly gained area between 2008 and 2012. Sectors C and D were the profile sections where the most sediment was lost from the profile between 2000 to 2008. However, sediment was regained in these sectors between 2008 and 2012. From 2000 to 2012 all sites except for UM14 saw a net increase in the area of sector A with the peak areal extent of sector A occurring in either 2008 or 2012 for most of the profiles. Finally, during the last time step of the survey period between 2012 and 2021, lake level rose rapidly to record-setting levels in 2020 before beginning to slightly decrease in 2021. Interestingly, all profiles except for UM21 saw a net increase in profile area between 2012 and

2021. Sectors B, C, and D all tended to increase in area during this time period. Concurrently, this period also saw the largest average drop in the area of sector A, as all sites lost beach sediments during this period with the notable exception of UM14 which gained area in sector A.

Overall, one of the primary observations of areal change throughout the study period was that at most sites sectors A and C tended to exhibit the most variability with areal changes in sector A usually being the opposite of those observed in sector C for any given period. Average areal trends in sectors B, C, and D, generally followed the same pattern as total profile areas, while the average areal trend in sector A followed a separate pattern. Sector A gained the most area when average lake levels were falling or were stable, while sectors B, C, and D tended to gain area during periods of rising lake level.

Nearshore Sediment Transport

MC Parameters and Classification

Table 4 summarizes key hydrodynamic parameters and the active zone limits of AC, ME, and SE conditions averaged across all study sites. Owing to substantially larger average H_s and H_e values, ME and SE conditions contain much more wave energy and have substantially larger R_2 and DOC values than AC conditions. The R_2 and DOC values are reported as heights and depths, respectively, from lake level.

Wave Parameter	AC	ME	SE
$\overline{H_s}$ (m)	0.22	0.82	2.49
$\overline{H_e}$ (m)	0.69	1.98	5.59
$\overline{T_p}$ (s)	3.26	4.52	7.28
$\overline{T_e}$ (s)	6.86	6.69	10.44
$\overline{R_2}$ (m)	0.08	0.23	0.62
$\overline{R_{2,e}}$ (m)	0.31	0.51	1.33
$\overline{DOC}$ (m)	0.47	1.63	4.84
$\overline{DOC_e}$ (m)	1.50	3.89	10.74

Table 4. *Averaged wave parameters and active zone limits for AC, ME, and SE MCs.* Displays the mean significant wave height (H_s), mean effective wave height (H_e), mean wave period (T_p), mean effective wave period (T_e), mean wave runup height (R_2), mean effective wave runup height ($R_{2,e}$), mean depth of closure (DOC), and mean effective depth of closure (DOC_e) for each morphodynamic condition considered in this paper.

Figure 8 illustrates the seasonal and monthly patterns of changes in the occurrence and relative dominance of each of the three classified MCs from data averaged across all six study sites and the corresponding monthly fluctuations in H_s values and lake levels. Throughout the entire study, AC conditions occurred 38.5% of the time, ME conditions occurred 58.0% of the time, SE conditions occurred 2.9% of the time, and calm conditions with no wave activity occurred the remaining 0.6% of the time.

a) Monthly MC Occurrence

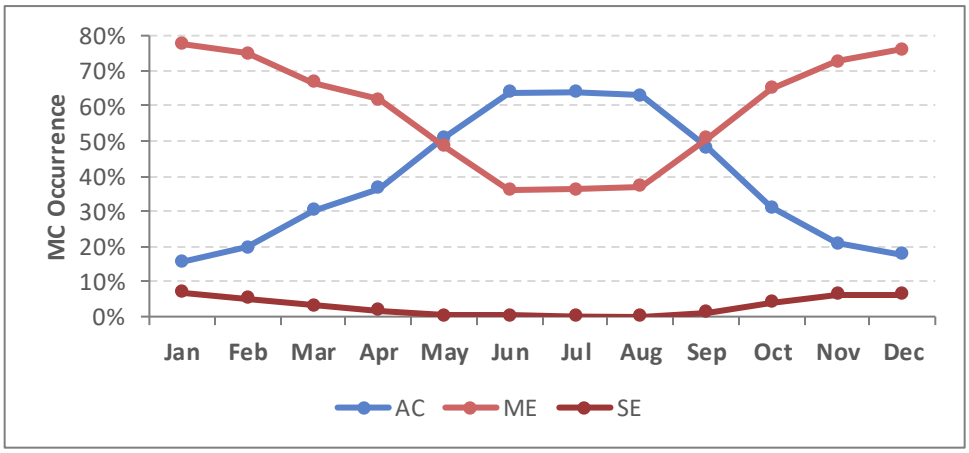

b) Mean Monthly Wave Height

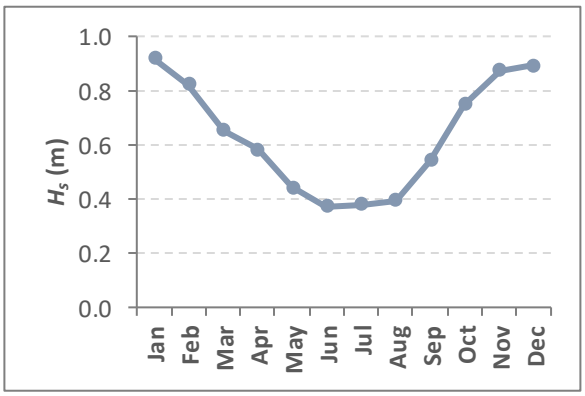

c) Mean Monthly Lake Level

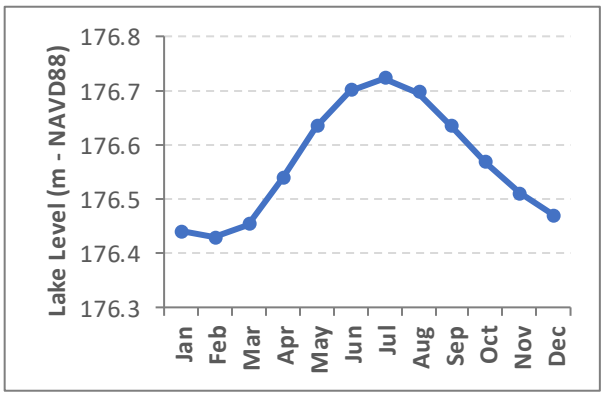

Figure 8. *Monthly variations in morphodynamic conditions, wave height, and lake level.* Data averaged across all six study sites shows marked seasonal variation in MCs, H_s, and lake level. a) Presents the seasonal patterns of all three MCs averaged across all study sites. b) – c) Demonstrate monthly fluctuations in two of the most important hydrodynamic variables which influence sediment transport: wave height and lake level.

AC conditions are the predominant MC during June, July, and August and drastically decrease into the fall, winter, and spring months. The rise in AC conditions exhibits the same trend as seasonal lake level fluctuations (Figure 8c), with the highest mean monthly lake levels occurring during the summer along with the highest rates of AC conditions. Conversely, ME and SE conditions have an inverse relationship with AC conditions and mean monthly lake level and have a noticeably direct relationship with mean monthly H_s values (Figure 8b, c). ME conditions

prevail over 60% of the time October through April. SE conditions, while rarer, also increase in frequency during the fall and winter months and are extremely rare during the summer months.

Roles of LS and CS Transport

Measurements of change in sector area were used to quantify the role that LS and CS sediment transport have in both interannual and decadal changes in profile morphology. Sites and survey periods dominated by LS processes generally have a wider range of total profile areal change and areal gains or losses in one cross-shore sector will not be balanced with a corresponding loss or gain, respectively, in another profile sector. Sites or survey periods dominated by CS processes will tend to maintain the same overall profile area with losses in one sector being compensated for by a corresponding gain in another sector. Figure 9 displays López-Dóriga & Ferreira's (2017) LvC index values for this study.

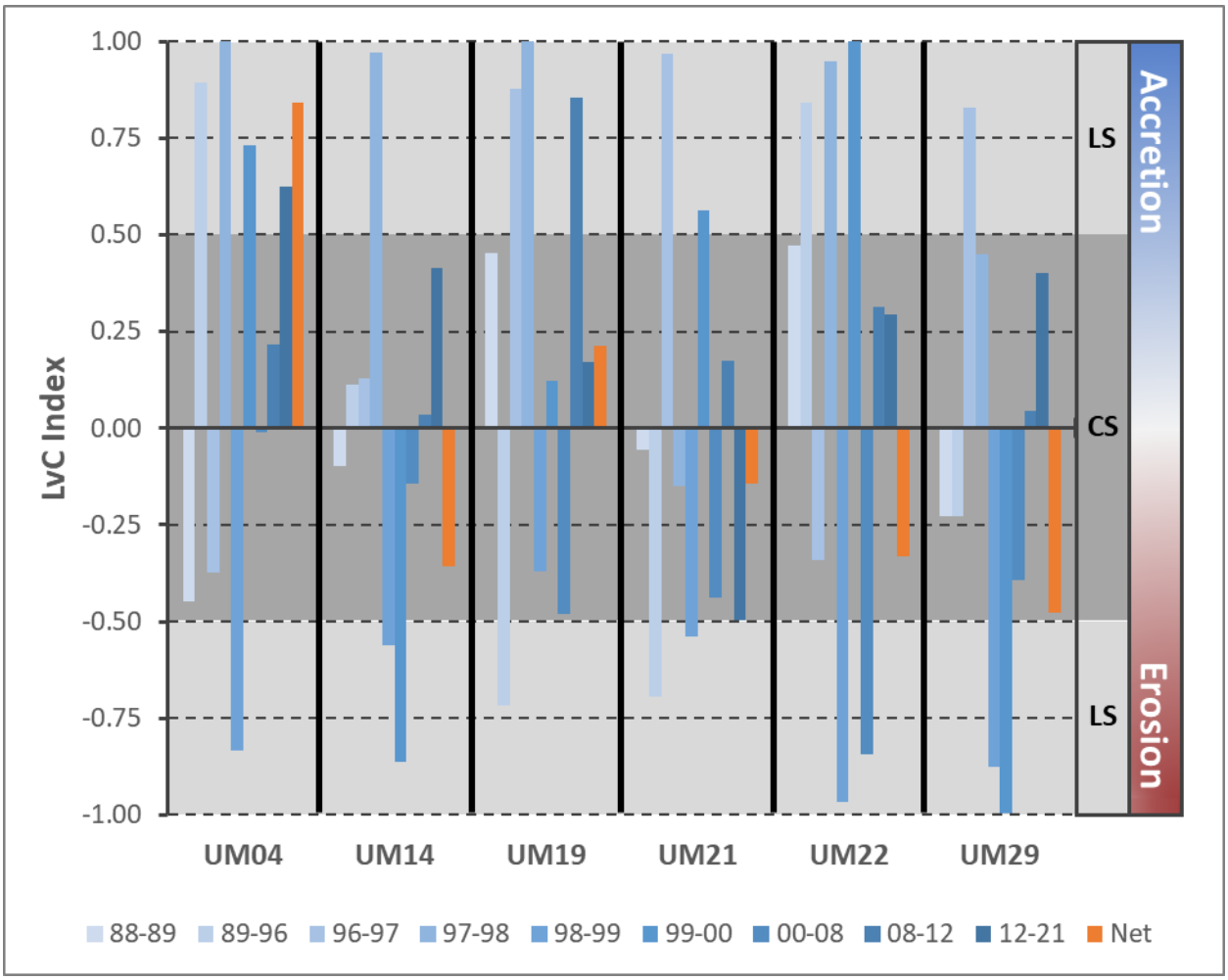

Figure 9. *Profile LvC index values, 1988 – 2021*. Displays the LvC index calculated using a modified version of Equation 2 from López-Dóriga & Ferreira (2017). The gray shading indicates whether a particular LvC index value reflects the dominance of LS or CS processes.

LvC index values exhibit a wide range of temporal variability across all study sites. While a majority of LvC values (55.5%) are between -0.5 and 0.5 and indicate a relative dominance of CS processes, all sites show large oscillations across the LvC index range, indicating fluctuations across time from dominance by erosive LS processes to dominance by accretionary LS processes. Despite periods of pronounced accretion or erosion due to LS transport, the net changes in profile area over the entire period for UM14, UM21, UM22, and UM29 indicate long-term dominance by CS processes with some erosion due to LS processes. At UM19, net changes in profile area reflect a dominance by CS processes with some accretion due

to LS processes. UM04 is the only study site where the net change in profile area indicates relative dominance by accretionary LS processes.

Analysis of hourly wave hindcast data during different MCs throughout the study period yields additional insight into the role of LS and CS sediment transport at each site. Table 5 displays the average wave direction, average angle of wave incidence, the average LS wave velocity vector magnitude, and the average CS wave velocity vector magnitude during AC, ME, and SE conditions. Positive and negative values for the LS velocity vector magnitude correspond to northward and southward directed motion, respectively. Positive and negative values for the CS velocity vector magnitude correspond to eastward and westward directed motion, respectively. Figure 10 displays the average wave vectors during AC, ME, and SE conditions.

MC	Wave Characteristics	UM04	UM14	UM19	UM21	UM22	UM29
AC	$\bar{\theta}$ (°)	341.52	290.01	296.32	293.15	293.15	278.75
	$\bar{\theta}_i$ (°)	76.48	49.99	54.68	47.85	47.85	68.75
	$LS\ \bar{v}$ (m/s)	-0.81	-1.72	-1.09	-1.23	-1.23	0.75
	$CS\ \bar{v}$ (m/s)	3.38	2.05	1.55	1.36	1.36	1.94
ME	$\bar{\theta}$ (°)	315.24	259.00	268.19	263.45	263.45	275.35
	$\bar{\theta}_i$ (°)	77.24	81.00	82.81	77.55	77.55	65.35
	$LS\ \bar{v}$ (m/s)	0.77	-0.64	-0.41	-0.74	-0.74	1.46
	$CS\ \bar{v}$ (m/s)	3.42	4.07	3.25	3.33	3.33	3.19
SE	$\bar{\theta}$ (°)	331.91	259.69	271.96	264.27	264.27	290.20
	$\bar{\theta}_i$ (°)	86.09	80.31	79.04	76.73	76.73	80.20
	$LS\ \bar{v}$ (m/s)	-0.74	-1.48	-1.22	-1.57	-1.57	1.22
	$CS\ \bar{v}$ (m/s)	10.85	8.66	6.30	6.65	6.65	7.04
Net LvC Index		0.84	-0.36	0.21	-0.14	-0.33	-0.48

Table 5. *Average wave directions and velocities associated with trends in LS/CS sediment transport.* Displays long-term averages of several key variables related to the dominance of LS and CS processes across the three morphodynamic conditions (MCs) at each study site. $\bar{\theta}$ is the average wave direction. $\bar{\theta}_i$ is the wave incidence angle. $LS\ \bar{v}$ is the mean LS wave velocity vector magnitude and $CS\ \bar{v}$ is the mean CS wave velocity vector magnitude.

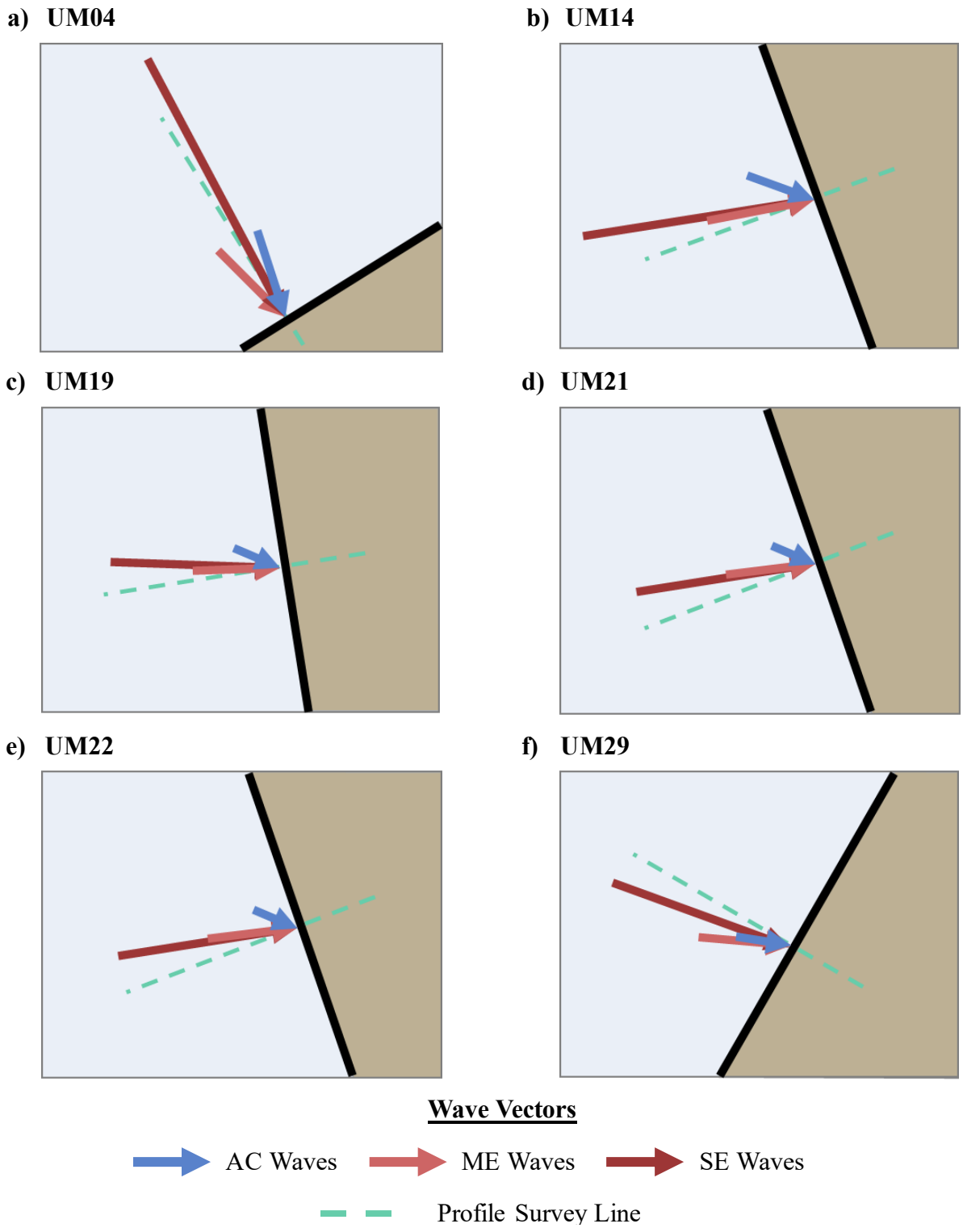

Figure 10. *Average wave vectors under different morphodynamic conditions.* The length of the arrows symbolizing the wave vectors corresponds to their relative magnitude. Overall, erosive waves tend to approach the shoreline at more direct perpendicular angles than accretionary waves.

With the exception of UM04, the angle of wave incidence is more oblique to the shoreline during AC conditions than during either ME or SE conditions. Consequently, the magnitudes of the LS and CS vectors are more closely matched during AC conditions indicating that LS transport likely has a more pronounced role in accretionary processes in the upper nearshore. During ME or SE conditions, waves tend to approach the shore at more direct angles, with no mean wave incidence angle being more than 25° from directly perpendicular to the shore for ME conditions and no more than 14° from directly perpendicular to the shore for SE conditions. These more direct angles of approach cause more wave energy to be directed in the CS direction during erosive wave conditions.

Sediment Mobility Across Profile Sectors

A final metric used to evaluate the role of different nearshore processes was a measure of the likelihood of sediment mobilization and transport during each MC within different profile sectors. Figure 11 displays the mean sediment mobilization likelihood by sector at each study site. On average, sediments in sector A can be mobilized by wave conditions 50.2% of the time, sediments in sector B can be mobilized 81.7% of the time, sediments in sector C can be mobilized 32.8% of the time, and sediments in sector D can be mobilized only 0.9% of the time. The vast difference in mobilization likelihood accounts for higher variability in profile elevations in sectors A through C and suggests that most sediment transport at any given location takes place well above the DOC_e for these study sites.

Due to a smaller range between DOC and R_2 limits, AC conditions predominately have the potential to initiate sediment transport in profile sectors A and B. Across all study sites, AC conditions only mobilize sediment in sector C an average of 1.5% of the time (Figure 11). In contrast to AC conditions, ME conditions are the most common set of conditions and also the

predominant conditions which mobilize sediment across sectors A, B, and C. Because of the greater wave heights associated with these conditions, a much greater portion of the profile can be mobilized by ME conditions than by AC conditions. SE conditions occur very rarely, but they are the only MC which can mobilize all profile sectors and the only MC able to mobilize sediment across the deeper portions of nearshore bars in sector C and on the outer profile slope in sector D.

Figure 12 shows an example with the 2021 profile from UM04 of how the calculated sediment mobility likelihood curves and the $\overline{DOC_e}$ and $\overline{R_{2,e}}$ limits for each MC can be used in tandem to depict regions of potential transport across profile sectors. Appendix D contains mean sediment mobilization likelihood graphs for each study site. At UM04, both the graphs of the AC mean sediment mobility rate (Figure 12a) and the AC active zone plotted on the 2021 profile (Figure 12b) indicate that accretionary waves generally only act on areas between 90-190 m lakeward from the survey benchmark. As was seen in Figure 11, AC conditions predominately mobilize sediment in sectors A and B. By contrast, ME conditions can mobilize sediment in sectors A, B, and C and SE conditions can mobilize sediment across all profile factors. However, sediment in sectors C and D is mobilized substantially less in comparison to sectors A and B and is typically mobilized only by wave conditions that are more likely to lead to erosion and net offshore transport of sediment.

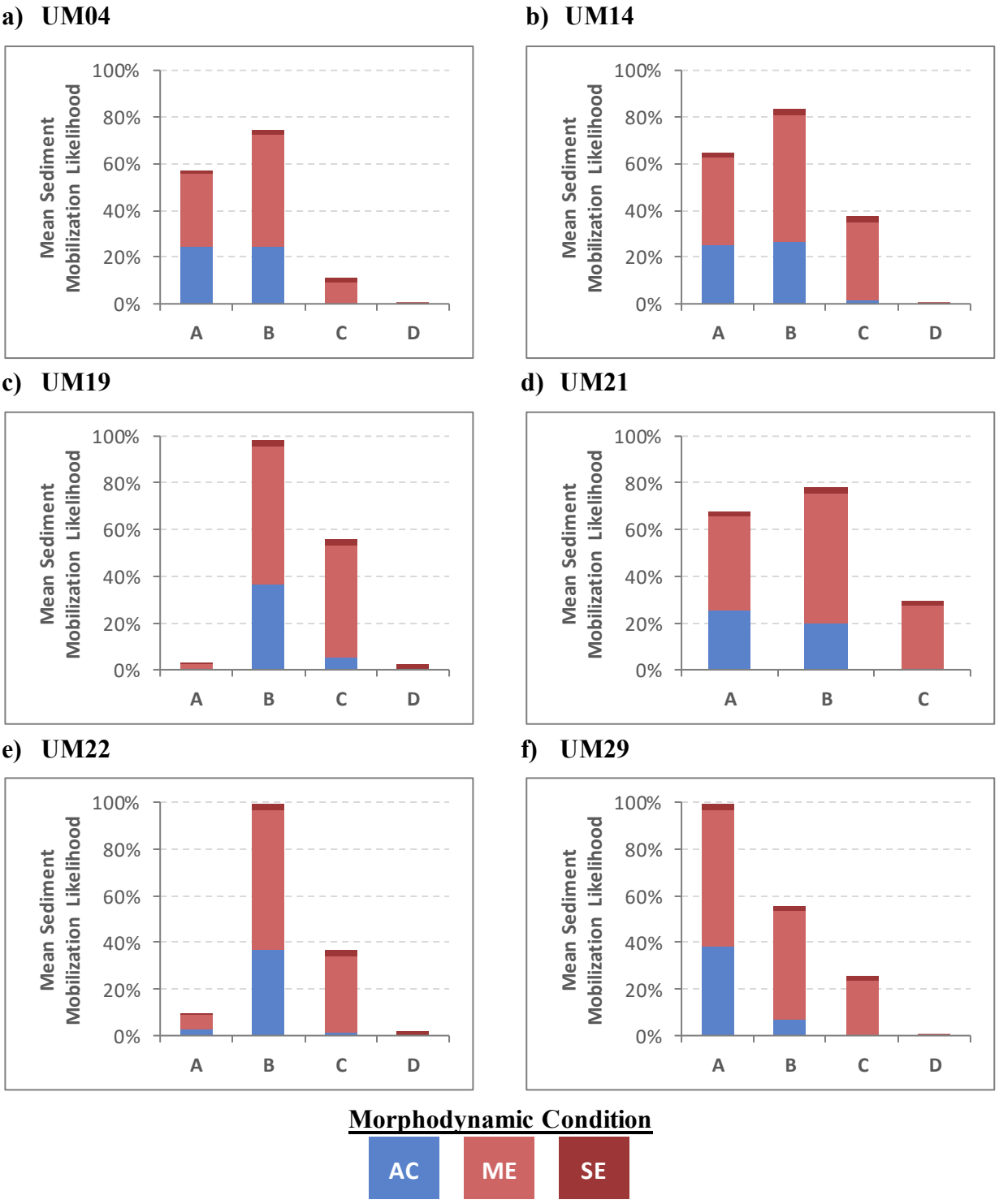

Figure 11. *Mean sediment mobilization likelihoods by profile sector.* Graphs show how often sediment within each profile sector under each MC. Because of the low magnitude of sediment mobilization potential in sector D at most sites, the bar is barely visible in a), b), e), and f).

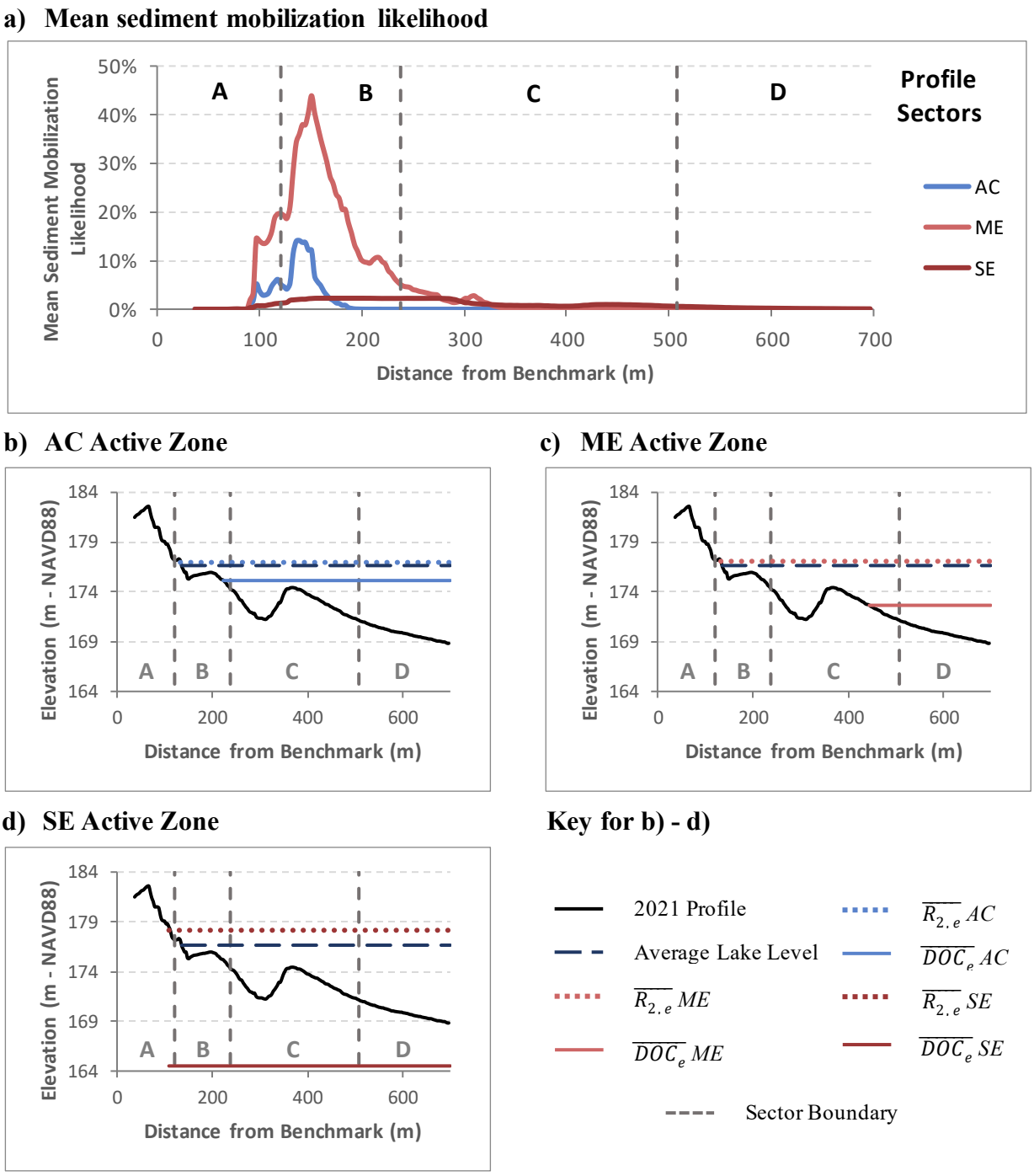

Figure 12. *UM04 mean sediment mobilization likelihood and active sediment transport zones, 2021.* Example from UM04 of how the three different MC states interact with and are distributed along observed profile morphology. a) Displays the mean sediment mobilization likelihood curves across all four profile sectors. b) – d) Display where those curves are located along the 2021 profile at UM04. Sediment within the active zone of each MC (between the effective DOC ($\overline{DOC_e}$) and the effective wave runup $\overline{R_{2,e}}$) has a high likelihood of being placed in suspension and transported when those conditions prevail throughout the year.

Discussion

The findings reported in this study quantitatively document relationships between nearshore sediment transport and potential beach recovery on the eastern coast of Lake Michigan on annual to decadal timescales. Unlike previous studies in the Great Lakes which have described individual aspects of beach and nearshore profile morphodynamics on hourly (Davis & Fox, 1972), event-scale (Greenwood et al., 2006; Houser & Greenwood, 2005b), monthly to seasonal (Dubois, 1973; Volpano et al., 2022; Weishar & Wood, 1983), or interannual (Davidson-Arnott, 1988; Davidson-Arnott & Bauer, 2021; Davis, 1976; Hands, 1976, 1979, 1981; Saylor & Hands, 1970; Theuerkauf et al., 2019) timescales, the primary focus of this study was on exploring multidecadal trends in sediment connectivity across morphologic zones. Beginning to address this knowledge gap will help to focus future coastal geomorphic change modelling efforts and to start to develop reasonable beach recovery predictions following periods of high lake level. The discussion will center around three key topics:

1) multidecadal trends in the relative roles of CS and LS sediment transport,

2) potential nearshore sediment sources for beach recovery, and

3) potential implications of these results for coastal management.

The Long-term Role of LS and CS Sediment Transport

Like most factors in coastal geomorphology, the relative importance of LS and CS components are both spatially and temporally variable. Taken together, the overall stability of profile areal measurements, the net LvC index values, the average wave incidence angles, and the LS and CS wave velocities during different MCs suggest that CS processes have a more dominant role in shaping the decadal evolution of profile morphology than LS processes at all study sites except for UM04.

While the net change in total profile area at UM04 exceeded 20% over the entire study period, the smaller net area changes of less than ±5.20% at all other study sites are indicative of relative stability in the coastal profile on decadal timescales associated with a balanced gradient of LS sediment transport (López-Dóriga & Ferreira, 2017). UM04's location immediately north and updrift of a harbor jetty is likely a major contributing factor to the observed multidecadal trend of accretion. Not only does the jetty act as a barrier to southerly-directed LS transport, but it also shields the beach from some of the erosive effects of ME conditions because ME waves at this site approach the profile from an off-perpendicular southerly incidence angle. The proximity of this site to a major human modification to the coastline in many ways makes UM04 an outlier among the other study sites which tends to exhibit intensified or different patterns of areal profile change.

While overall profile areas remained relatively stable at most of the study sites over the slightly more than three decades of monitoring, changes in sector and subsector areas fluctuated widely between surveys. Changes in the area of profile sectors exhibited long-term patterns which appear to be closely associated with fluctuations in lake level (Figure 7). The large variability in interannual LvC index values at most sites (Figure 9) is indicative of shifts in the dominance of LS and CS processes across time. However, for all sites except UM04, the LvC index calculated using the net areal change between 1988 and 2021 reflected a multidecadal trend of the dominance of CS transport. This suggests that all sites except UM04 have a stronger CS sediment connectivity over several decades, while the profile at UM04 has a stronger LS sediment connectivity than CS sediment connectivity.

A final piece of evidence indicating the long-term dominance of CS transport at most of the study sites is the shore-perpendicular wave approach angle during ME and SE conditions and

the associated LS and CS wave velocities. Erosive wave conditions generally exert a stronger control over the CS form of profile morphology than accretionary wave conditions (Thom & Hall, 1991). When ME and SE waves approach a beach at a nearly 90° angle, there is little wave refraction during wave breaking and most of the wave energy is dissipated directly onto the beach, resulting in a stronger undertow that pulls sediment lakeward. Because of the more perpendicular wave incidence angles during ME and SE conditions, the magnitude of the average CS wave velocities are often 3 to 10 times the magnitude of average LS wave velocities (Table 5). Taken together, these results indicate most of the erosive energy that reworks profile morphology occurs in the CS direction as opposed to the LS direction.

While CS processes may be the primary factor shaping long-term changes in profile morphology, it is essential to note that wave incident angles associated with LS and CS wave velocities during AC conditions do not follow the same patterns as ME and SE conditions. AC waves tend to approach at an oblique angle to the shore. Consequently, the relative magnitudes of average AC LS and CS wave velocities are similar. However, UM04 and UM29 do not follow this pattern. At both sites, the AC wave incidence angle is less oblique than the other four study sites (Table 5, Figure 10). The magnitude of CS wave velocities at UM04 and UM29 during AC conditions is much greater than the magnitude of LS wave velocities. Interestingly, the LvC index values of these two sites show the greatest long-term trend of the dominance of LS processes. This is counter-intuitive, as it would make sense to assume that sites with more perpendicular average angles of wave incidence should display a greater dominance of CS processes. Both UM04 and UM29 have been modified through human activity and coastal armoring which likely causes profile behavior to deviate from an anticipated outcome.

Nearshore Sediment Sources for Beach Recovery

One of the most impactful uses of the results of this study is to assess the location of potential sources of nearshore sediment for beach recovery following periods of high lake level. By quantifying where and how often AC, ME, and SE conditions have the potential to mobilize sediment across the coastal profile, it is possible to assess the likelihood that sediment from one part of the profile can be transported lakeward during the MCs known to lead to onshore-directed sediment transport and beach accretion. The long-term nature of the assessment of this study is crucial because it allows for improved insight into overall trends in beach and nearshore morphology and improved insight into sediment connectivity between different profile sectors over multiple cycles of rising and falling lake levels.

While the general concept of varying hydrodynamic conditions shifting the upper and lower limits of the active zone of the profile has been explored in previous studies (e.g., Meadows et al., 1997), the ability to quantify exactly where along the profile the active zone occurs with different types of MCs without the use of a more complex numerical model allows for powerful insight into the role of different nearshore sectors in beach erosion and recovery. Given the results of this study, it appears that these profiles have a greater degree of sediment connectivity related to offshore-directed sediment transport than onshore-directed sediment transport. Under AC conditions, usually only sediment from sectors A and B can be transported onshore. However, under erosive conditions sediments from all profile sectors can be mobilized and transported offshore. As a result, if sediment is eroded from sector A and carried CS and deposited in sector C, there is very little likelihood that sediment will be able to make its way back onto the beach.

Consequently, it is highly unlikely that much of the sediment stored in deeper nearshore bars in sector C or in the lower shoreface in sector D can serve as a source for beach accretion over management-relevant timescales of 1-5 years. However, the nearshore bars in sector C are well within the activation limits of ME and SE conditions and likely serve as decadal sinks for eroded material from the beach and the inner nearshore swash bar. These findings suggest that not only are shallow nearshore sediments essential for short-term beach recovery following storms (Evans, 1939; Hands, 1984; Houser, 2009; Morton et al., 1994; M. S. Phillips et al., 2015, 2017), but they may also be the most important source of sediment for long-term beach recovery following periods of accelerated erosion during high lake levels. While the nearshore bars may not be a source of sediment for beach accretion, nearshore bars do still play an important morphodynamic role in protecting accretionary gains in beach sediment by causing larger waves to break and dissipating wave energy which protects beach sediment from direct exposure to the most energetic wave conditions.

There are other potential mechanisms besides the ones used to classify AC conditions in this study which could lead to onshore transport of nearshore bar sediment such as velocity and acceleration skewness and infragravity waves (Aagaard & Greenwood, 1994; Elgar et al., 2001; Hoefel & Elgar, 2003). However, these alternate mechanisms have highly site-specific impacts and are difficult to parameterize quantitatively.

In general, AC conditions do not have the potential to mobilize sediment from sector C in a manner which would meaningfully contribute to beach accretion or dune growth. The site with the highest potential rate of onshore transport under AC conditions in sector C was UM19, which had a potential sediment movement rate of 5.2%. Given the dominance of ME conditions in this sector, this amount of AC time is likely too short to contribute meaningfully to beach accretion or

dune growth. While Olson (1958) originally speculated that nearshore bars had an important role to play in dune growth by dissipating wave energy and serving as a source of sediment for onshore-directed transport, it is doubtful sediment from sector C would serve as a major source of sediment for dune growth along Great Lakes shorelines. The maximum measured profile areas in sector A at most study sites occurred during the 2008 and 2012 surveys when lake levels remained below average levels for an extended period of time. As a result of increased sediment supply and longer beach widths, more sediment was likely available for aeolian transport and dune building processes between 2000 and 2012. However, lake level would likely have to drop farther down than the anomalous low levels observed between 2000 and 2012 and remain at lower levels, instead of rising rapidly as they did between 2013 and 2020, for sediments located in nearshore bars to be able to be mobilized by AC conditions and transported onto the beach where the sediment could then be transported via aeolian processes into coastal dunes. Investigating other potential mechanisms for the onshore-directed transport of nearshore and lower shoreface sediments onto the beach and into dunes will likely remain a critical research area in the future (Aagaard et al., 2004; Anthony & Aagaard, 2020).

Implications for Coastal Management

Mitigating the impacts of shoreline erosion is often the primary goal for coastal zone management (Dobie et al., 2022; Lawrence, 1997; Smith & Houser, 2022). Historically, the dominant strategy to combat coastal erosion and protect infrastructure in the Great Lakes has been to harden or armor the shoreline through the use of seawalls, jetties, groins, and rip-rap revetments (Clark et al., 2013; Lino Grima, 1993; Rovey & Borucki, 1994). Periods of high lake level and accelerated coastal erosion, such as those experienced from 1985 to 1986 and from 2013 to 2020, are associated with an increased number of shoreline stabilization and armoring

projects (Department of Environment, Great Lakes, and Energy, 2021; House, 2020). While these structures can slow erosion in the near-term, shoreline armoring interrupts natural sediment transport gradients by decreasing the amount of sediment available for transport in littoral drift and accelerating erosion at the base and along the edges of the armored structure (Branham et al., 2021; Ewing, 2015; Kittinger & Ayers, 2010; Lin & Wu, 2014; Scyphers et al., 2020; Wood, 1988).

A decrease in sediment availability in LS littoral drift and the scouring of the lakebed at the base of seawalls and revetments is likely to limit future rates of beach recovery. A decrease in sediment availability via littoral drift will substantially reduce a key sediment source for AC waves in sector B and consequently slow the rate of beach accretion during calm conditions. Additionally, because hardened coastal structures reflect incident wave energy downward towards the lakebed instead of dissipating it over a more gently sloped shoreface, the lakebed at the base of the structure is eroded at an accelerated rate. Deepening of this area of the profile would further decrease the amount of time AC waves could mobilize sediment for onshore-directed sediment transport because the sediment in the upper nearshore in sector B would be much closer to the DOC_e limit for AC conditions. By reducing the total sediment able to be mobilized during AC conditions through modifying LS littoral sediment drift and lowering the elevation of the inner nearshore swash bar, the current prevailing strategy to manage coastal erosion could be facilitating more severe erosion in the future.

Conclusion

The methods developed in this study hold promise for future applications in other regions of the Great Lakes or on marine coasts for scalable quantitative assessments of coastal morphodynamics and sediment connectivity. These methods are more accessible than complex numerical modeling approaches and can be applied in any location with a series of profile observations and contemporaneous wave hindcast and water level records. Some possible directions for future research aimed at predicting beach recovery include advancing the knowledge of swash zone morphodynamics, quantifying how much sediment eroded from the beach during erosive conditions is deposited within the inner nearshore swash bar and thus mobilizable during onshore transport under accretionary conditions, and studying how the CS displacement of nearshore bars may support beach recovery through dissipating incoming wave energy by shifting the location of the breaker line for high-energy waves farther offshore.

The findings of this study are an important initial step toward better understanding multidecadal patterns of beach and nearshore sediment transport and sediment connectivity across the coastal profile in the Great Lakes. Identifying the long-term boundaries of the active zones of different MCs allows for unique and powerful insight into the role of different profile zones in beach erosion and accretion. While sediment transport is ultimately the result of LS and CS processes working in tandem, CS processes appear to drive most of the long-term changes in profile morphology at the sites examined in this study. This finding suggests that future modeling studies of beach erosion and recovery should particularly focus on CS sediment transport patterns. Although sediment from the subaerial beach can be eroded and deposited offshore in the swash bar, in nearshore bars, or beyond nearshore bars towards the lake basin, only sediment contained in very shallow swash bars and storm ridges in the inner nearshore can meaningfully

contribute to near-term and long-term beach recovery. While onshore and offshore migration of nearshore bars was documented throughout the study period, they rarely became shallow enough to serve as a direct source of sediment for beach recovery during accretionary wave conditions. As a result, the vast amount of sediment stored within or lakeward of nearshore bars during periods of accelerated erosion associated with high lake levels is likely out of play for future beach recovery without a dramatic drop in lake levels. These findings provide quantitative confirmation of the critical importance of inner nearshore swash zone sediments and processes in beach recovery.

Given the importance of swash zone sediment transport for beach recovery, this study also highlights how increased coastal armoring throughout the study area could impact beach recovery in the future. Decreasing sediment transport via littoral drift in the inner nearshore and deepening the profile in front of armored coastlines via increased wave scour will decrease sediment availability within the active zone for accretionary conditions which lead to onshore-directed sediment transport. These changes will likely lead to slower beach recovery rates which will increase future coastal vulnerability to erosive events and further endanger existing coastal infrastructure. To protect the ecological and socio-economic value of eastern Lake Michigan's sandy beaches, researchers, coastal managers, and property owners need to begin to consider and plan for a future where beach recovery following periods of elevated lake level will be much slower or perhaps not even possible in some areas due to extensive armoring.

REFERENCES

Aagaard, T. (2014). Sediment supply to beaches: Cross-shore sand transport on the lower shoreface. *Journal of Geophysical Research: Earth Surface*, *119*(4), 913–926. https://doi.org/10.1002/2013JF003041

Aagaard, T., Black, K. P., & Greenwood, B. (2002). Cross-shore suspended sediment transport in the surf zone: A field-based parameterization. *Marine Geology*, *185*(3), 283–302. https://doi.org/10.1016/S0025-3227(02)00193-7

Aagaard, T., Davidson-Arnott, R., Greenwood, B., & Nielsen, J. (2004). Sediment supply from shoreface to dunes: Linking sediment transport measurements and long-term morphological evolution. *Geomorphology*, *60*(1), 205–224. https://doi.org/10.1016/j.geomorph.2003.08.002

Aagaard, T., & Greenwood, B. (1994). Suspended sediment transport and the role of infragravity waves in a barred surf zone. *Marine Geology*, *118*(1–2), 23–48. https://doi.org/10.1016/0025-3227(94)90111-2

Aagaard, T., & Greenwood, B. (1995). Suspended sediment transport and morphological response on a dissipative beach. *Continental Shelf Research*, *15*(9), 1061–1086. https://doi.org/10.1016/0278-4343(94)00068-X

Aagaard, T., Kroon, A., Hughes, M. G., & Greenwood, B. (2008). Field observations of nearshore bar formation. *Earth Surface Processes and Landforms*, *33*(7), 1021–1032. https://doi.org/10.1002/esp.1599

Abdelhady, H. U., & Troy, C. D. (2023). A reduced-complexity shoreline model for coastal areas with large water level fluctuations. *Coastal Engineering*, *179*, 104249. https://doi.org/10.1016/j.coastaleng.2022.104249

Ahrens, J. P. (2000). A fall-velocity equation. *Journal of Waterway, Port, Coastal, and Ocean Engineering*, *126*(2), 99–102. https://doi.org/10.1061/(ASCE)0733-950X(2000)126:2(99)

Almeida, L. P., Ferreira, Ó., & Pacheco, A. (2011). Thresholds for morphological changes on an exposed sandy beach as a function of wave height. *Earth Surface Processes and Landforms*, *36*(4), 523–532. https://doi.org/10.1002/esp.2072

Amin, S. M. N., & Davidson-Arnott, R. G. D. (1995). Toe erosion of glacial till bluffs: Lake Erie south shore. *Canadian Journal of Earth Sciences*, *32*(7), 829–837. https://doi.org/10.1139/e95-069

Anderson, O., Harrison, A., Heumann, B., Godwin, C., & Uzarski, D. (2023). The influence of extreme water levels on coastal wetland extent across the Laurentian Great Lakes. *Science of The Total Environment*, *885*, 163755. https://doi.org/10.1016/j.scitotenv.2023.163755

Angel, J. R. (1995). Large-scale storm damage on the U.S. shores of the Great Lakes. *Journal of Great Lakes Research*, *21*(3), 287–293. https://doi.org/10.1016/S0380-1330(95)71039-5

Anthony, E. J., & Aagaard, T. (2020). The lower shoreface: Morphodynamics and sediment connectivity with the upper shoreface and beach. *Earth-Science Reviews*, *210*, 103334. https://doi.org/10.1016/j.earscirev.2020.103334

Arbogast, A. F., & Loope, W. L. (1999). Maximum-limiting ages of Lake Michigan coastal dunes: Their correlation with Holocene lake level history. *Journal of Great Lakes Research*, *25*(2), 372–382. https://doi.org/10.1016/S0380-1330(99)70746-X

Arbogast, A. F., Lovis, W. A., McKeehan, K. G., & Monaghan, G. W. (2023). A 5500-year record of coastal dune evolution along the shores of Lake Michigan in the North American Great Lakes: The relationship of lake-level fluctuations and climate. *Quaternary Science Reviews*, *307*, 108042. https://doi.org/10.1016/j.quascirev.2023.108042

Ashton, A. D., & Murray, A. B. (2006). *High-angle wave instability and emergent shoreline shapes: 2. Wave climate analysis and comparisons to nature*. https://doi.org/10.1029/2005JF000423

Aubrey, D. G. (1979). Seasonal patterns of onshore/offshore sediment movement. *Journal of Geophysical Research: Oceans*, *84*(C10), 6347–6354. https://doi.org/10.1029/JC084iC10p06347

Bajorunas, L., & Duane, D. B. (1967). Shifting offshore bars and harbor shoaling. *Journal of Geophysical Research (1896-1977)*, *72*(24), 6195–6205. https://doi.org/10.1029/JZ072i024p06195

Battjes, J. A. (1974). Surf similarity. *Coastal Engineering 1974*, 466–480. https://doi.org/10.1061/9780872621138.029

Bird, E. C. F. (1983). Factors influencing beach erosion and accretion: A global review. In A. McLachlan & T. Erasmus (Eds.), *Sandy beaches as ecosystems: Based on the proceedings of the First International Symposium on Sandy Beaches, held in Port Elizabeth, South Africa, 17–21 January 1983* (Vol. 19, pp. 709–717). Springer Netherlands. https://doi.org/10.1007/978-94-017-2938-3_57

Birkemeier, W. A. (1981). *Coastal changes, eastern Lake Michigan, 1970-74* (Miscellaneous Report MR 81-2; p. 89). U.S. Army, Corps of Engineers, Coastal Engineering Research Center. https://apps.dtic.mil/sti/pdfs/ADA097985.pdf

Birkemeier, W. A. (1985). Field data on seaward limit of profile change. *Journal of Waterway, Port, Coastal, and Ocean Engineering*, *111*(3), 598–602. https://doi.org/10.1061/(ASCE)0733-950X(1985)111:3(598)

Boczar-Karakiewicz, B., & Davidson-Arnott, R. G. D. (1987). Nearshore bar formation by non-linear wave processes—A comparison of model results and field data. *Marine Geology*, *77*(3), 287–304. https://doi.org/10.1016/0025-3227(87)90118-6

Bosboom, J., & Stive, M. J. F. (2023). *Coastal dynamics* (1.2). Delft University of Technology. https://textbooks.open.tudelft.nl/textbooks/catalog/book/37

Branham, J., Onda, K., Kaza, N., BenDor, T. K., & Salvesen, D. (2021). How does the removal of federal subsidies affect investment in coastal protection infrastructure? *Land Use Policy*, *102*, 105245. https://doi.org/10.1016/j.landusepol.2020.105245

Brutsché, K. E., Iii, J. R., Pollock, C. E., & McFall, B. C. (2016). *Calculating depth of closure using WIS hindcast data* (Technical Note CHETN-VI-45; Coastal and Hydraulics Engineering Technical Note, p. 9). U.S. Army Corps of Engineers, U.S. Army Engineer Research and Development Center [Coastal and Hydraulics Laboratory]. https://usace.contentdm.oclc.org/digital/collection/p266001coll1/id/4109/

Butt, T., & Russell, P. (2000). Hydrodynamics and cross-shore sediment transport in the swash-zone of natural beaches: A review. *Journal of Coastal Research*, *16*(2), 255–268.

Clark, G., Brose, B., & Cox, J. (2013). *Great Lakes coastal shore protection structures and their effects on coastal processes* (p. 6). University of Wisconsin Sea Grant Institute & Water Resources Institute. https://publications.aqua.wisc.edu/product/great-lakes-coastal-shore-protection-structures-and-their-effects-on-coastal-processes/

Coastal Engineering Research Center. (1984). *Shore protection manual: Volume I* (p. 639). Department of the Army, Waterways Experiment Station, Corps of Engineers.

Corbella, S., & Stretch, D. D. (2012). Shoreline recovery from storms on the east coast of Southern Africa. *Natural Hazards and Earth System Sciences*, *12*(1), 11–22. https://doi.org/10.5194/nhess-12-11-2012

Davidson-Arnott, R. G. D. (1988). Controls on formation and form of barred nearshore profiles. *Geographical Review*, *78*(2), 185–193. https://doi.org/10.2307/214176

Davidson-Arnott, R. G. D., & Bauer, B. O. (2021). Controls on the geomorphic response of beach-dune systems to water level rise. *Journal of Great Lakes Research*, *47*(6), 1594–1612. https://doi.org/10.1016/j.jglr.2021.05.006

Davis, R. A. (1976). *Coastal changes, eastern Lake Michigan, 1970-73* (Technical Paper TP 76-16; p. 64). U.S. Army Corps of Engineers, Coastal Engineering Research Center. https://erdc-library.erdc.dren.mil/jspui/bitstream/11681/22733/1/CERC%20Technical%20Paper%20No%2076-16.pdf

Davis, R. A., & Fox, W. T. (1972). Coastal processes and nearshore sand bars. *Journal of Sedimentary Research*, *42*(2), 401–412. https://doi.org/10.1306/74D72568-2B21-11D7-8648000102C1865D

Davis, R. A., Fox, W. T., Hayes, M. O., & Boothroyd, J. C. (1972). Comparison of ridge and runnel systems in tidal and non-tidal environments. *SEPM Journal of Sedimentary Research*, *Vol. 42*. https://doi.org/10.1306/74D7256D-2B21-11D7-8648000102C1865D

Deacu, D., Fortin, V., Klyszejko, E., Spence, C., & Blanken, P. D. (2012). Predicting the net basin supply to the Great Lakes with a hydrometeorological model. *Journal of Hydrometeorology*, *13*(6), 1739–1759. https://doi.org/10.1175/JHM-D-11-0151.1

Dean, R. G. (1973). Heuristic models of sand transport in the surf zone. *First Australian Conference on Coastal Engineering, 1973: Engineering Dynamics of the Coastal Zone*, 215–221. https://doi.org/10.3316/informit.971703171672500

Department of Environment, Great Lakes, and Energy. (2021, January 5). *2020 By the Numbers: 2,284 shoreline permits issued*. https://www.michigan.gov/egle/newsroom/mi-environment/2021/01/05/2020-by-the-numbers-2284-shoreline-permits-issued

Dobie, S., Doran, P. J., Norton, R. K., Hughes, S., & Goode, M. J. (2022). Defining coastal resilience in the Great Lakes: A systematic review and critical comparison. *Journal of Great Lakes Research*, *48*(6), 1361–1374. https://doi.org/10.1016/j.jglr.2022.08.001

Dubarbier, B., Castelle, B., Marieu, V., & Ruessink, G. (2015). Process-based modeling of cross-shore sandbar behavior. *Coastal Engineering*, *95*, 35–50. https://doi.org/10.1016/j.coastaleng.2014.09.004

Dubois, R. N. (1973). Seasonal variation of a limnic beach. *Geological Society of America Bulletin*, *84*(5), 1817–1824. https://doi.org/10.1130/0016-7606(1973)84<1817:SVOALB>2.0.CO;2

Dubois, R. N. (1975). Support and refinement of the Bruun Rule on beach erosion. *The Journal of Geology*, *83*(5), 651–657.

Dyhr-Nielsen, M., & Sørensen, T. (1970). Some sand transport phenomena on coasts with bars. *Coastal Engineering 1970*, 855–865. https://doi.org/10.1061/9780872620285.054

Eichentopf, S., Cáceres, I., & Alsina, J. M. (2018). Breaker bar morphodynamics under erosive and accretive wave conditions in large-scale experiments. *Coastal Engineering*, *138*, 36–48. https://doi.org/10.1016/j.coastaleng.2018.04.010

Eichentopf, S., van der Zanden, J., Cáceres, I., Baldock, T. E., & Alsina, J. M. (2020). Influence of storm sequencing on breaker bar and shoreline evolution in large-scale experiments. *Coastal Engineering*, *157*, 103659. https://doi.org/10.1016/j.coastaleng.2020.103659

Elfrink, B., & Baldock, T. (2002). Hydrodynamics and sediment transport in the swash zone: A review and perspectives. *Coastal Engineering*, *45*(3), 149–167. https://doi.org/10.1016/S0378-3839(02)00032-7

Elgar, S., Gallagher, E. L., & Guza, R. T. (2001). Nearshore sandbar migration. *Journal of Geophysical Research: Oceans*, *106*(C6), 11623–11627. https://doi.org/10.1029/2000JC000389

Environmental Systems Research Institute. (2021). *ArcGIS Pro* (2.9.0) [Computer software]. Environmental Systems Research Institute. https://www.esri.com/en-us/arcgis/products/arcgis-pro/overview

Evans, O. F. (1939). Mass transportation of sediments on subaqueous terraces. *The Journal of Geology*, *47*(3), 325–334.

Evans, O. F. (1940). The low and ball of the eastern shore of Lake Michigan. *The Journal of Geology*, *48*(5), 476–511.

Evtimova, V. V., & Donohue, I. (2016). Water-level fluctuations regulate the structure and functioning of natural lakes. *Freshwater Biology*, *61*(2), 251–264. https://doi.org/10.1111/fwb.12699

Ewing, L. C. (2015). Resilience from coastal protection. *Philosophical Transactions of the Royal Society A: Mathematical, Physical and Engineering Sciences*, *373*(2053), 20140383. https://doi.org/10.1098/rsta.2014.0383

Farhadzadeh, A., Ghazian, M., & Bokuniewicz, H. (2018). Contribution of seiche to beach profile evolution in eastern Lake Erie. *Shore and Beach*, *86*(2), 19–26.

Fingleton, W. G. (1973). *A study of shore erosion at seventeen sites along eastern Lake Michigan* [Masters Thesis, Western Michigan University]. https://scholarworks.wmich.edu/cgi/viewcontent.cgi?article=3665&context=masters_theses

Fox, W. T., & Davis, R. A. (1973). Simulation model for storm cycles and beach erosion on Lake Michigan. *Geological Society of America Bulletin*, *84*(5), 1769–1790. https://doi.org/10.1130/0016-7606(1973)84<1769:SMFSCA>2.0.CO;2

Gallagher, E. L., Elgar, S., & Guza, R. T. (1998). Observations of sand bar evolution on a natural beach. *Journal of Geophysical Research: Oceans*, *103*(C2), 3203–3215. https://doi.org/10.1029/97JC02765

Gomes da Silva, P., Coco, G., Garnier, R., & Klein, A. H. F. (2020). On the prediction of runup, setup and swash on beaches. *Earth-Science Reviews*, *204*, 103148. https://doi.org/10.1016/j.earscirev.2020.103148

Gorman, L., Morang, A., & Larson, R. (1998). Monitoring the coastal environment; Part IV: Mapping, shoreline changes, and bathymetric analysis. *Journal of Coastal Research*, *14*(1), 61–92.

Greenwood, B., Permanand-Schwartz, A., & Houser, C. A. (2006). Emergence and migration of a nearshore bar: Sediment flux and morphological change on a multi-barred beach in the Great Lakes. *Géographie Physique et Quaternaire*, *60*(1), 31–47. https://doi.org/10.7202/016363ar

Gronewold, A. D., Bruxer, J., Durnford, D., Smith, J. P., Clites, A. H., Seglenieks, F., Qian, S. S., Hunter, T. S., & Fortin, V. (2016). Hydrological drivers of record-setting water level rise on Earth's largest lake system. *Water Resources Research*, *52*(5), 4026–4042. https://doi.org/10.1002/2015WR018209

Gronewold, A. D., Fortin, V., Lofgren, B., Clites, A., Stow, C. A., & Quinn, F. (2013). Coasts, water levels, and climate change: A Great Lakes perspective. *Climatic Change*, *120*(4), 697–711. https://doi.org/10.1007/s10584-013-0840-2

Gronewold, A. D., & Rood, R. B. (2019). Recent water level changes across Earth's largest lake system and implications for future variability. *Journal of Great Lakes Research*, *45*(1), 1–3. https://doi.org/10.1016/j.jglr.2018.10.012

Grossmann, F., Hurther, D., Sánchez-Arcilla, A., & Alsina, J. M. (2023). Influence of the initial beach profile on the sediment transport processes during post-storm onshore bar migration. *Journal of Geophysical Research: Oceans*, *128*(4), 17. https://doi.org/10.1029/2022JC019299

Grossmann, F., Hurther, D., van der Zanden, J., Cáceres, I., Sánchez-Arcilla, A., & Alsina, J. M. (2022). Near-bed sediment transport during offshore bar migration in large-scale experiments. *Journal of Geophysical Research: Oceans*, *127*(5), e2021JC017756. https://doi.org/10.1029/2021JC017756

Grossmann, F., Hurther, D., van der Zanden, J., Sánchez-Arcilla, A., & Alsina, J. M. (2023). Near-bed sediment transport processes during onshore bar migration in large-scale experiments: Comparison with offshore bar migration. *Journal of Geophysical Research: Oceans*, *128*(3), e2022JC018998. https://doi.org/10.1029/2022JC018998

Hallermeier, R. J. (1978). Uses for a calculated limit depth to beach erosion. *Coastal Engineering Proceedings*, *16*, Article 16. https://doi.org/10.9753/icce.v16.88

Hallermeier, R. J. (1981). A profile zonation for seasonal sand beaches from wave climate. *Coastal Engineering*, *4*, 253–277. https://doi.org/10.1016/0378-3839(80)90022-8

Hamblin, P. F. (1987). Meteorological forcing and water level fluctuations on Lake Erie. *Journal of Great Lakes Research*, *13*(4), 436–453. https://doi.org/10.1016/S0380-1330(87)71665-7

Hands, E. B. (1976). *Observations of barred coastal profiles under the influence of rising water levels, Eastern Lake Michigan, 1967-71* (Technical Report TR 76-1; p. 113). U.S. Army Corps of Engineers, Coastal Engineering Research Center. https://hdl.handle.net/11681/12598

Hands, E. B. (1979). *Changes in rates of shore retreat, Lake Michigan, 1967-76* (Technical Paper TP 79-4; p. 71). U.S. Army Corps of Engineers, Coastal Engineering Research Center. https://ia600308.us.archive.org/1/items/changesinratesof00hand/changesinratesof00hand_bw.pdf

Hands, E. B. (1980). *Prediction of shore retreat and nearshore profile adjustments to rising water levels on the Great Lakes* (Technical Paper TP 80-7; p. 119). U.S. Army Corps of Engineers, Coastal Engineering Research Center. https://hdl.handle.net/11681/22181

Hands, E. B. (1981). *Predicting adjustments in shore and offshore sand profiles on the Great Lakes* (Coastal Engineering Technical Aid CETA 81-4; p. 25). U.S. Army Corps of Engineers, Coastal Engineering Research Center. https://archive.org/details/predictingadjust00hand/page/n31/mode/2up

Hands, E. B. (1984). *The Great Lakes as a test model for profile response to sea level changes* (Miscellaneous Paper CERC-84-14; p. 26). U.S. Army Corps of Engineers, Coastal Engineering Research Center. https://apps.dtic.mil/sti/pdfs/ADA153062.pdf

Hoefel, F., & Elgar, S. (2003). Wave-induced sediment transport and sandbar migration. *Science*, *299*(5614), 1885–1887. https://doi.org/10.1126/science.1081448

House, K. (2020, July 17). Michigan's coast is being armored with seawalls, making erosion worse. *Bridge Michigan*. https://www.bridgemi.com/michigan-environment-watch/michigans-coast-being-armored-seawalls-making-erosion-worse

Houser, C. (2009). Synchronization of transport and supply in beach-dune interaction. *Progress in Physical Geography: Earth and Environment*, *33*(6), 733–746. https://doi.org/10.1177/0309133309350120

Houser, C., & Greenwood, B. (2005a). Hydrodynamics and sediment transport within the inner surf zone of a lacustrine multiple-barred nearshore. *Marine Geology*, *218*(1), 37–63. https://doi.org/10.1016/j.margeo.2005.02.029

Houser, C., & Greenwood, B. (2005b). Profile response of a lacustrine multiple barred nearshore to a sequence of storm events. *Geomorphology*, *69*(1), 118–137. https://doi.org/10.1016/j.geomorph.2004.12.005

Houser, C., & Greenwood, B. (2007). Onshore migration of a swash bar during a storm. *Journal of Coastal Research*, *2007*(231), 1–14. https://doi.org/10.2112/03-0135.1

Huang, C., Zhu, L., Ma, G., Meadows, G. A., & Xue, P. (2021). Wave climate associated with changing water level and ice cover in Lake Michigan. *Frontiers in Marine Science*, *8*. https://www.frontiersin.org/articles/10.3389/fmars.2021.746916

International Joint Commission. (2012). *Lake Superior regulation: Addressing uncertainty in upper Great Lakes water levels: Final report to the International Joint Commission* (International Upper Great Lakes Study, p. 215). https://ijc.org/en/glam/lake-superior-regulation-addressing-uncertainty-upper-great-lakes-water-levels

Iribarren, C. R., & Nogales, M. C. (1949). Protection des ports, Section II, Comm. 4. *XVIIth International Navigation Congress*, 31–80. https://repository.tudelft.nl/islandora/object/uuid%3A7ab718ff-a74d-4141-8c3f-413044c751c4

Joint Airborne Lidar Bathymetry Technical Center of eXpertise (JALBTCX). (2022a). *2008 U.S. Army Corps of Engineers (USACE) National Coastal Mapping Program (NCMP) topobathy LiDAR DEM: Lake Michigan* [GeoTIFF]. NOAA Office for Coastal Management. https://www.fisheries.noaa.gov/inport/item/50072

Joint Airborne Lidar Bathymetry Technical Center of eXpertise (JALBTCX). (2022b). *2012 U.S. Army Corps of Engineers (USACE) National Coastal Mapping Program (NCMP) topobathy LiDAR DEM: Lake Michigan (MI, WI)* [GeoTIFF]. NOAA Office for Coastal Management. https://www.fisheries.noaa.gov/inport/item/64407

Kayastha, M. B., Ye, X., Huang, C., & Xue, P. (2022). Future rise of the Great Lakes water levels under climate change. *Journal of Hydrology*, *612*, 128205. https://doi.org/10.1016/j.jhydrol.2022.128205

Keddy, P. A., & Reznicek, A. A. (1986). Great Lakes vegetation dynamics: The role of fluctuating water levels and buried seeds. *Journal of Great Lakes Research*, *12*(1), 25–36. https://doi.org/10.1016/S0380-1330(86)71697-3

Kilibarda, Z., & Kilibarda, V. (2022). Foredune and beach dynamics on the southern shores of Lake Michigan during recent high water levels. *Geosciences*, *12*(4), Article 4. https://doi.org/10.3390/geosciences12040151

King, C. A. M. (1970). Feedback relationships in geomorphology. *Geografiska Annaler: Series A, Physical Geography*, *52*(3–4), 147–159. https://doi.org/10.1080/04353676.1970.11879820

Kittinger, J. N., & Ayers, A. L. (2010). Shoreline armoring, risk management, and coastal resilience under rising seas. *Coastal Management*, *38*(6), 634–653. https://doi.org/10.1080/08920753.2010.529038

Kobayashi, N., & Jung, H. (2012). Beach erosion and recovery. *Journal of Waterway, Port, Coastal, and Ocean Engineering*, *138*(6), 473–483. https://doi.org/10.1061/(ASCE)WW.1943-5460.0000147

Krueger, R., Zoet, L. K., & Rawling III, J. E. (2020). Coastal bluff evolution in response to a rapid rise in surface water level. *Journal of Geophysical Research: Earth Surface*, *125*(10), e2019JF005428. https://doi.org/10.1029/2019JF005428

Larson, G., & Schaetzl, R. (2001). Origin and evolution of the Great Lakes. *Journal of Great Lakes Research*, *27*(4), 518–546. https://doi.org/10.1016/S0380-1330(01)70665-X

Larson, M., & Kraus, N. C. (1995). Prediction of cross-shore sediment transport at different spatial and temporal scales. *Marine Geology*, *126*(1), 111–127. https://doi.org/10.1016/0025-3227(95)00068-A

Lawrence, P. L. (1997). Integrated coastal zone management and the Great Lakes. *Land Use Policy*, *14*(2), 119–136. https://doi.org/10.1016/S0264-8377(96)00039-7

Lenters, J. D. (2001). Long-term trends in the seasonal cycle of Great Lakes water levels. *Journal of Great Lakes Research*, *27*(3), 342–353. https://doi.org/10.1016/S0380-1330(01)70650-8

Lick, W., Lick, J., & Ziegler, C. K. (1994). The resuspension and transport of fine-grained sediments in Lake Erie. *Journal of Great Lakes Research*, *20*(4), 599–612. https://doi.org/10.1016/S0380-1330(94)71181-3

Lin, Y.-T., & Wu, C. H. (2014). A field study of nearshore environmental changes in response to newly-built coastal structures in Lake Michigan. *Journal of Great Lakes Research*, *40*(1), 102–114. https://doi.org/10.1016/j.jglr.2013.12.013

Lino Grima, A. P. (1993). Enhancing resilience in Great Lakes water levels management. *International Journal of Environmental Studies*, *44*(2–3), 97–111. https://doi.org/10.1080/00207239308710853

López, I., Pagán, J. I., Navarro-González, F. J., Müller, G. V., & Aragonés, L. (2020). Determination of the study period necessary for calculating the equilibrium beach profile and the depth of closure. *Applied Ocean Research*, *94*, 102005. https://doi.org/10.1016/j.apor.2019.102005

López-Dóriga, U., & Ferreira, Ó. (2017). Longshore and cross-shore morphological variability of a berm–bar system under low to moderate wave energy. *Journal of Coastal Research*, *33*(5), 1161–1171. https://doi.org/10.2112/JCOASTRES-D-16-00050.1

Marinho, B., Coelho, C., Larson, M., & Hanson, H. (2020). Cross-shore modelling of multiple nearshore bars at a decadal scale. *Coastal Engineering*, *159*, 103722. https://doi.org/10.1016/j.coastaleng.2020.103722

Mattheus, C. R., Braun, K. N., Theuerkauf, E. J., & Santoro, J. A. (2022). Urban pocket-beach morphodynamics along the wave-dominated southwest coast of Lake Michigan: An analysis of shoreline and sand volumetric changes. *Journal of Great Lakes Research*, *48*(1), 52–67. https://doi.org/10.1016/j.jglr.2021.10.009

Mattheus, C. R., Diggins, T. P., Boyce, C., Cockrell, J., Kruske, M., & VanWinkle, M. (2019). Geomorphology of a harbor-breakwater beach along a high sand-supply, wave-dominated Great Lakes littoral cell. *Journal of Coastal Research*, *35*(1), 41–55. https://doi.org/10.2112/JCOASTRES-D-17-00209.1

McGlashan, D. J., Duck, R. W., & Reid, C. T. (2005). Defining the foreshore: Coastal geomorphology and British laws. *Estuarine, Coastal and Shelf Science*, *62*(1), 183–192. https://doi.org/10.1016/j.ecss.2004.08.016

Meadows, G. A., Meadows, L. A., Wood, W. L., Hubertz, J. M., & Perlin, M. (1997). The relationship between Great Lakes water levels, wave energies, and shoreline damage. *Bulletin of the American Meteorological Society*, *78*(4), 675–684. https://doi.org/10.1175/1520-0477(1997)078<0675:TRBGLW>2.0.CO;2

Microsoft. (2023). *Microsoft® Excel® for Microsoft 365 MSO* (Version 2307) [Computer software]. Microsoft.

Morisawa, M., & King, C. A. M. (1974). Monitoring the coastal environment. *Geology*, *2*(8), 385. https://doi.org/10.1130/0091-7613(1974)2<385:MTCE>2.0.CO;2

Mortimer, C. H. (1988). Discoveries and testable hypotheses arising from Coastal Zone Color Scanner imagery of southern Lake Michigan. *Limnology and Oceanography*, *33*(2), 203–226. https://doi.org/10.4319/lo.1988.33.2.0203

Morton, R. A., Paine, J. G., & Gibeaut, J. C. (1994). Stages and durations of post-storm beach recovery, southeastern Texas coast, U.S.A. *Journal of Coastal Research*, *10*(4), 884–908.

National Oceanic and Atmospheric Administration, National Geodetic Survey. (2018). *IGLD 85 height conversion*. https://www.ngs.noaa.gov/TOOLS/

National Oceanic and Atmospheric Administration, National Ocean Service. (2023). *Coastal water temperature guide* [dataset]. NOAA National Centers for Environmental Information. https://www.ncei.noaa.gov/products/coastal-water-temperature-guide

National Oceanic and Atmospheric Administration, National Ocean Service, Center for Operational Oceanographic Products and Services. (2023a). *Verified hourly heights at 9087023, Ludington, MI* [dataset]. https://tidesandcurrents.noaa.gov/stationhome.html?id=9087023

National Oceanic and Atmospheric Administration, National Ocean Service, Center for Operational Oceanographic Products and Services. (2023b). *Verified hourly heights at 9087031, Holland, MI* [dataset]. https://tidesandcurrents.noaa.gov/stationhome.html?id=9087031

Nicholls, R. J., Larson, M., Capobianco, M., & Birkemeier, W. A. (1999). Depth of closure: Improving understanding and prediction. *Coastal Engineering 1998*, 2888–2901. https://doi.org/10.1061/9780784404119.219

Norton, R. K., Meadows, L. A., & Meadows, G. A. (2011). Drawing lines in law books and on sandy beaches: Marking ordinary high water on Michigan's Great Lakes shorelines under the Public Trust Doctrine. *Coastal Management*, *39*(2), 133–157. https://doi.org/10.1080/08920753.2010.540709

Olson, J. S. (1958). Lake Michigan dune development. 3. Lake-level, beach, and dune oscillations. *The Journal of Geology*, *66*(5), 473–483.

Olyphant, G. A., & Bennett, S. W. (1994). Contemporary and historical rates of eolian sand transport in the Indiana Dunes area of southern Lake Michigan. *Journal of Great Lakes Research*, *20*(1), 153–162. https://doi.org/10.1016/S0380-1330(94)71137-0

Osborne, P. D., & Greenwood, B. (1992). Frequency dependent cross-shore suspended sediment transport. 2. A barred shoreface. *Marine Geology*, *106*(1), 25–51. https://doi.org/10.1016/0025-3227(92)90053-K

Pape, L., Plant, N. G., & Ruessink, B. G. (2010). On cross-shore migration and equilibrium states of nearshore sandbars. *Journal of Geophysical Research: Earth Surface*, *115*(F3). https://doi.org/10.1029/2009JF001501

Phillips, M. R., & Jones, A. L. (2006). Erosion and tourism infrastructure in the coastal zone: Problems, consequences and management. *Tourism Management*, *27*(3), 517–524. https://doi.org/10.1016/j.tourman.2005.10.019

Phillips, M. S., Harley, M. D., Turner, I. L., Splinter, K. D., & Cox, R. J. (2017). Shoreline recovery on wave-dominated sandy coastlines: The role of sandbar morphodynamics and nearshore wave parameters. *Marine Geology*, *385*, 146–159. https://doi.org/10.1016/j.margeo.2017.01.005

Phillips, M. S., Turner, I. L., Cox, R. J., Splinter, K. D., & Harley, M. D. (2015). Will the sand come back? Observations and characteristics of beach recovery. *Coasts & Ports 2015*, 7. https://www.researchgate.net/publication/282314389_Will_the_sand_come_back_Observations_and_characteristics_of_beach_recovery

Pilkey, O. H., & Cooper, J. A. G. (2002). Longshore transport volumes: A critical view. *Journal of Coastal Research*, *36*(sp1), 572–580. https://doi.org/10.2112/1551-5036-36.sp1.572

Plant, N. G., Freilich, M. H., & Holman, R. A. (2001). Role of morphologic feedback in surf zone sandbar response. *Journal of Geophysical Research: Oceans*, *106*(C1), 973–989. https://doi.org/10.1029/2000JC900144

Plant, N. G., Holman, R. A., Freilich, M. H., & Birkemeier, W. A. (1999). A simple model for interannual sandbar behavior. *Journal of Geophysical Research: Oceans*, *104*(C7), 15755–15776. Scopus. https://doi.org/10.1029/1999jc900112

Pranzini, E., & Williams, A. T. (2021). The equilibrium concept, or…(mis)concept in beaches. *Geosciences*, *11*(2), 59. https://doi.org/10.3390/geosciences11020059

Quinn, F. H. (2002). Secular changes in Great Lakes water level seasonal cycles. *Journal of Great Lakes Research*, *28*(3), 451–465. https://doi.org/10.1016/S0380-1330(02)70597-2

R Core Team. (2023). *R: A language and environment for statistical computing* (4.1.2) [R]. R Foundation for Statistical Computing. https://www.R-project.org/

Roelvink, J. A., & Brøker, I. (1993). Cross-shore profile models. *Coastal Engineering*, *21*(1), 163–191. https://doi.org/10.1016/0378-3839(93)90049-E

Rovey, C. W., & Borucki, M. K. (1994). Bluff evolution and long-term recession rates, southwestern Lake Michigan. *Environmental Geology*, *23*(4), 256–263. https://doi.org/10.1007/BF00766740

Ruessink, B. G., Houwman, K. T., & Hoekstra, P. (1998). The systematic contribution of transporting mechanisms to the cross-shore sediment transport in water depths of 3 to 9 m. *Marine Geology*, *152*(4), 295–324. https://doi.org/10.1016/S0025-3227(98)00133-9

Ruessink, B. G., Houwman, K. T., & Hoekstra, P. (1999). Medium-term frequency distributions of cross-shore suspended sediment transport rates in water depths of 3 to 9 m. *Coastal Engineering*, *38*(1), 25–46. https://doi.org/10.1016/S0378-3839(99)00023-X

Ruessink, B. G., & Terwindt, J. H. J. (2000). The behaviour of nearshore bars on the time scale of years: A conceptual model. *Marine Geology*, *163*(1), 289–302. https://doi.org/10.1016/S0025-3227(99)00094-8

Ruggiero, P., Walstra, D. J. R., Gelfenbaum, G., & van Ormondt, M. (2009). Seasonal-scale nearshore morphological evolution: Field observations and numerical modeling. *Coastal Engineering*, *56*(11), 1153–1172. https://doi.org/10.1016/j.coastaleng.2009.08.003

Sallenger, A. H., Holman, R. A., & Birkemeier, W. A. (1985). Storm-induced response of a nearshore-bar system. *Marine Geology*, *64*(3), 237–257. https://doi.org/10.1016/0025-3227(85)90107-0

Sanchez-Arcilla, A., & Caceres, I. (2018). An analysis of nearshore profile and bar development under large scale erosive and accretive waves. *Journal of Hydraulic Research*, *56*(2), 231–244. https://doi.org/10.1080/00221686.2017.1315748

Saylor, J. H., & Hands, E. B. (1970). Properties of longshore bars in the Great Lakes. *Coastal Engineering Proceedings*, *1*(12), Article 53. https://doi.org/10.9753/icce.v12.53

Schauberger, P., & Walker, A. (2023). *openxlsx: Read, write and edit xlsx files* (4.2.5.2) [R]. https://CRAN.R-project.org/package=openxlsx

Scyphers, S. B., Beck, M. W., Furman, K. L., Haner, J., Keeler, A. G., Landry, C. E., O'Donnell, K. L., Webb, B. M., & Grabowski, J. H. (2020). Designing effective incentives for living shorelines as a habitat conservation strategy along residential coasts. *Conservation Letters*, *13*(5), e12744. https://doi.org/10.1111/conl.12744

Short, A. D. (1979). Three dimensional beach-stage model. *The Journal of Geology*, *87*(5), 553–571.

Smith, A., & Houser, C. (2022). Perspectives on Great Lakes coastal management: A case study of the Point Pelee foreland, Canada. *Ocean & Coastal Management*, *228*, 106329. https://doi.org/10.1016/j.ocecoaman.2022.106329

Splinter, K. D., & Coco, G. (2021). Challenges and opportunities in coastal shoreline prediction. *Frontiers in Marine Science*, *8*. https://doi.org/10.3389/fmars.2021.788657

Splinter, K. D., Turner, I. L., & Davidson, M. A. (2013). How much data is enough? The importance of morphological sampling interval and duration for calibration of empirical shoreline models. *Coastal Engineering*, *77*, 14–27. https://doi.org/10.1016/j.coastaleng.2013.02.009

Stive, M. J. F., De Vriend, H. J., Nicholls, R. J., & Capobianco, M. (1993). Shore nourishment and the active zone: A time scale dependent view. *Coastal Engineering 1992*, 2464–2473. https://doi.org/10.1061/9780872629332.188

Stockberger, M. T., & Wood, W. L. (1991). Application of equilibrium beach concepts to sandy Great Lakes profiles. *Coastal Engineering 1990*, 2291–2303. https://doi.org/10.1061/9780872627765.175

Stockdon, H. F., Holman, R. A., Howd, P. A., & Sallenger, A. H. (2006). Empirical parameterization of setup, swash, and runup. *Coastal Engineering*, *53*(7), 573–588. https://doi.org/10.1016/j.coastaleng.2005.12.005

Sunamura, T., & Horikawa, K. (1974). Two dimensional beach transformation due to waves. *Coastal Engineering 1974*, 920–938. https://doi.org/10.1061/9780872621138.056

Tanner, W. F. (1975). Beach processes, Berrien County, Michigan. *Journal of Great Lakes Research*, *1*(1), 171–178. https://doi.org/10.1016/S0380-1330(75)72344-4

Theuerkauf, E. J., & Braun, K. N. (2021). Rapid water level rise drives unprecedented coastal habitat loss along the Great Lakes of North America. *Journal of Great Lakes Research*, *47*(4), 945–954. https://doi.org/10.1016/j.jglr.2021.05.004

Theuerkauf, E. J., Braun, K. N., Nelson, D. M., Kaplan, M., Vivirito, S., & Williams, J. D. (2019). Coastal geomorphic response to seasonal water-level rise in the Laurentian Great Lakes: An example from Illinois Beach State Park, USA. *Journal of Great Lakes Research*, *45*(6), 1055–1068. https://doi.org/10.1016/j.jglr.2019.09.012

Theuerkauf, E. J., Meadows, G. A., & Meadows, L. A. (2022). Improving coastal resilience planning with respect to long-term water level fluctuations by examining decadal coastal profile behavior at sandy, harbor filet beaches along Lake Michigan in the Great Lakes of North America. *Shore & Beach*, *90*(3), 36–43. https://doi.org/10.34237/1009034

Thom, B. G., & Hall, W. (1991). Behaviour of beach profiles during accretion and erosion dominated periods. *Earth Surface Processes and Landforms*, *16*(2), 113–127. https://doi.org/10.1002/esp.3290160203

Thompson, T. A. (1992). Beach-ridge development and lake-level variation in southern Lake Michigan. *Sedimentary Geology*, *80*(3–4), 305–318. https://doi.org/10.1016/0037-0738(92)90048-V

Thompson, T. A., & Baedke, S. J. (1995). Beach-ridge development in Lake Michigan: Shoreline behavior in response to quasi-periodic lake-level events. *Marine Geology*, *129*(1), 163–174. https://doi.org/10.1016/0025-3227(95)00110-7

Thompson, T. A., & Baedke, S. J. (1997). Strand-plain evidence for late Holocene lake-level variations in Lake Michigan. *Geological Society of America Bulletin*, *109*(6), 666–682. https://doi.org/10.1130/0016-7606(1997)109<0666:SPEFLH>2.3.CO;2

Trebitz, A. S. (2006). Characterizing seiche and tide-driven daily water level fluctuations affecting coastal ecosystems of the Great Lakes. *Journal of Great Lakes Research*, *32*(1), 102–116. https://doi.org/10.3394/0380-1330(2006)32[102:CSATDW]2.0.CO;2

Troy, C. D., Cheng, Y.-T., Lin, Y.-C., & Habib, A. (2021). Rapid lake Michigan shoreline changes revealed by UAV LiDAR surveys. *Coastal Engineering*, *170*, 104008. https://doi.org/10.1016/j.coastaleng.2021.104008

U.S. Army Corps of Engineers. (2023). *Wave Information Study (WIS)* [dataset]. https://wis.erdc.dren.mil/

Vallejo, L. E., & Degroot, R. (1988). Bluff response to wave action. *Engineering Geology*, *26*(1), 1–16. https://doi.org/10.1016/0013-7952(88)90003-8

van der Meulen, T., & Gourlay, M. R. (1968). Beach and dune erosion tests. In *Coastal Engineering 1968* (Vol. 1, pp. 701–707). American Society of Civil Engineers. https://ascelibrary.org/doi/book/10.1061/9780872620131 10.1061/9780872620131

van Dijk, D. (2021). Foredune dynamics at a Lake Michigan site during rising and high lake levels. *Journal of Great Lakes Research*, *47*(6), 1581–1593. https://doi.org/10.1016/j.jglr.2021.10.012

van Rijn, L. C., Tonnon, P. K., & Walstra, D. J. R. (2011). Numerical modelling of erosion and accretion of plane sloping beaches at different scales. *Coastal Engineering*, *58*(7), 637–655. https://doi.org/10.1016/j.coastaleng.2011.01.009

Volpano, C. A., Zoet, L. K., Rawling, J. E., & Theuerkauf, E. J. (2022). Measuring and modelling nearshore recovery of an eroded beach in Lake Michigan, USA. *Journal of Great Lakes Research*, *48*(3), 633–644. https://doi.org/10.1016/j.jglr.2022.03.012

Volpano, C. A., Zoet, L. K., Rawling, J. E., Theuerkauf, E. J., & Krueger, R. (2020). Three-dimensional bluff evolution in response to seasonal fluctuations in Great Lakes water levels. *Journal of Great Lakes Research*, *46*(6), 1533–1543. https://doi.org/10.1016/j.jglr.2020.08.017

Weishar, L. L., & Wood, W. L. (1983). An evaluation of offshore and beach changes on a tideless coast. *Journal of Sedimentary Research*, *53*(3), 847–858. https://doi.org/10.1306/212F82D3-2B24-11D7-8648000102C1865D

Wickham, H. (2011). The split-apply-combine strategy for data analysis. *Journal of Statistical Software*, *40*, 1–29. https://doi.org/10.18637/jss.v040.i01

Wickham, H. (2021). *tidyr: Tidy messy data* (1.1.4) [Computer software]. Posit PBC. https://CRAN.R-project.org/package=tidyr

Wickham, H., & Bryan, J. (2023). *readxl: Read Excel files* (1.4.2) [R]. Posit PBC. https://CRAN.R-project.org/package=readxl

Wickham, H., François, R., Henry, L., & Müller, K. (2021). *dplyr: A grammar of data manipulation* (1.0.7) [R]. Posit PBC. https://CRAN.R-project.org/package=dplyr

Wijnberg, K. M., & Kroon, A. (2002). Barred beaches. *Geomorphology*, *48*(1), 103–120. https://doi.org/10.1016/S0169-555X(02)00177-0

Wilcox, D. A. (2004). Implications of hydrologic variability on the succession of plants in Great Lakes wetlands. *Aquatic Ecosystem Health & Management*, *7*(2), 223–231. https://doi.org/10.1080/14634980490461579

Wood, W. L. (1988). Effects of seawalls on profile adjustment along Great Lakes coastlines. *Journal of Coastal Research*, 135–146.

Wood, W. L., Todd Stockberger, M., & Madalon, L. J. (1994). Modeling beach and nearshore profile response to lake level change. *Journal of Great Lakes Research*, *20*(1), 206–214. https://doi.org/10.1016/S0380-1330(94)71141-2

Wood, W. L., & Weishar, L. L. (1984). Beach response to long period lake-level variation. *Proceedings 19th Coastal Engineering Conference*, 1571–1583. https://doi.org/10.1061/9780872624382.108

Wright, L. D., & Short, A. D. (1984). Morphodynamic variability of surf zones and beaches: A synthesis. *Marine Geology*, *56*(1–4), 93–118. https://doi.org/10.1016/0025-3227(84)90008-2

Wright, L. D., Short, A. D., & Green, M. O. (1985). Short-term changes in the morphodynamic states of beaches and surf zones: An empirical predictive model. *Marine Geology*, *62*(3), 339–364. https://doi.org/10.1016/0025-3227(85)90123-9

Zuzek, P. J., Nairn, R. B., & Thieme, S. J. (2003). Spatial and temporal considerations for calculating shoreline change rates in the Great Lakes basin. *Journal of Coastal Research*, *38*, 125–146.

APPENDIX A: WAVE INFORMATION STUDY STATION INFORMATION

Site ID	Primary Station ID	Primary Station Latitude (°N)	Primary Station Longitude (°W)	Primary Station Water Depth (m)	Primary Station Distance Offshore from Survey Benchmark (km)	Secondary Station IDs	Missing Hourly Records (1988-2021)
UM04	94456	41.88	86.80	29	9.74	94449, 94450, 94450, 94453, 94454, 94457, 94459, 94462, 94463, 94466, 94467	3.58%
UM14	94413	43.12	86.36	39	6.93	94408, 94409, 94410, 94411, 94412, 94413, 94414, 94415, 94416, 94417	2.79%
UM19	94387	43.92	86.52	23	5.73	94383, 94384, 94385, 94386, 94388, 94389	1.95%
UM21	94386	43.96	86.52	16	4.75	94383, 94384, 94385, 94387, 94388, 94389	1.95%
UM22	94386	43.96	86.52	16	4.73	94383, 94384, 94385, 94387, 94388, 94389	1.95%
UM29	94372	44.32	86.36	30	4.96	94368, 94369, 94370, 94371, 94373, 94374, 94375, 94376	1.68%

Table 6. *Wave Information Study (WIS) station information*. Table provides additional details for the WIS station data used in this study. Hourly records between 1/1/1988 and 12/31/2021 were downloaded for all primary and secondary stations. Gaps in the records of the primary station were filled using the average of available data from secondary stations adjacent to the primary station for each study site. The "Missing Hourly Records (1988-2021)" column shows the percentage of hourly records still missing at each site after using this technique to fill gaps in the primary station record.

APPENDIX B: EXAMPLE OF CLIPPED COASTAL PROFILES

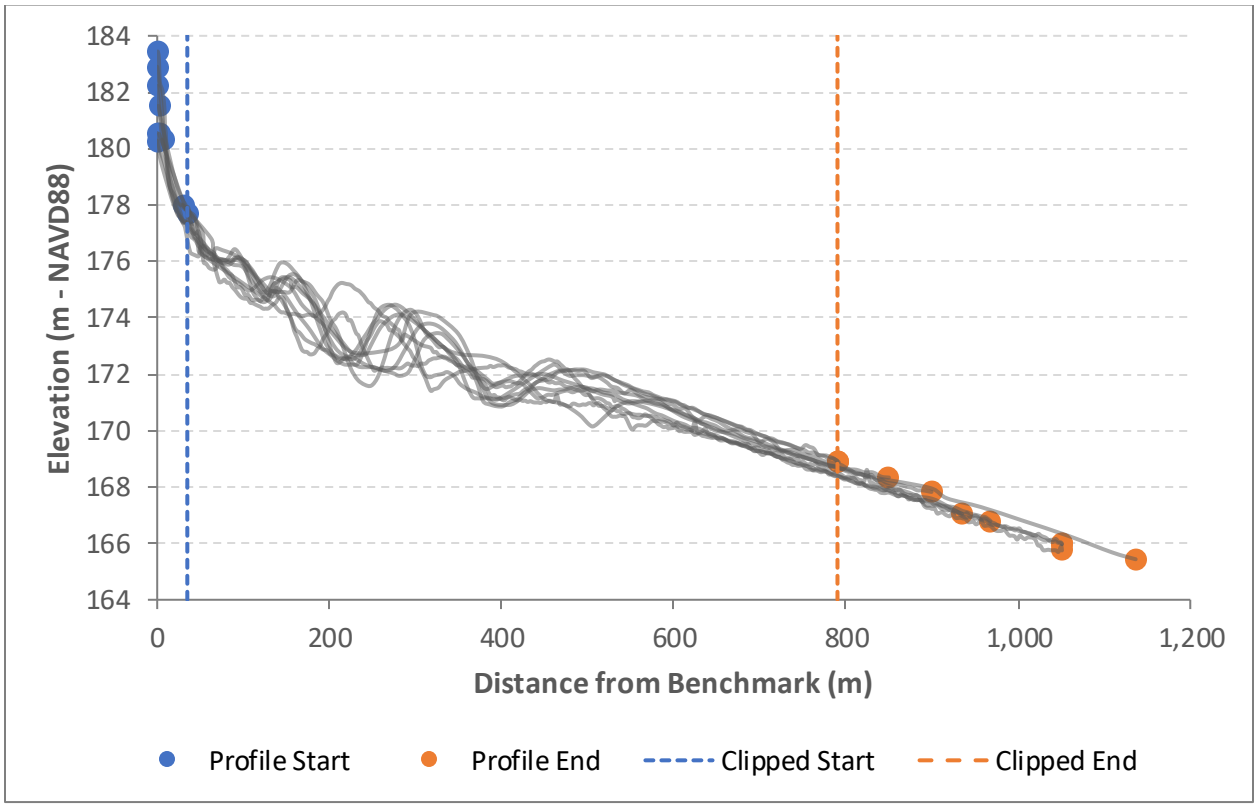

Figure 13. *Example of unclipped and clipped profile extents from UM14.* Displays the full length of all ten coastal profiles surveyed at UM14. Profiles were clipped to their maximum shared common extent to ensure data comparability across the entire study period.

APPENDIX C: PROFILE SECTOR AND SUBSECTOR CLASSIFICATION

a) UM04

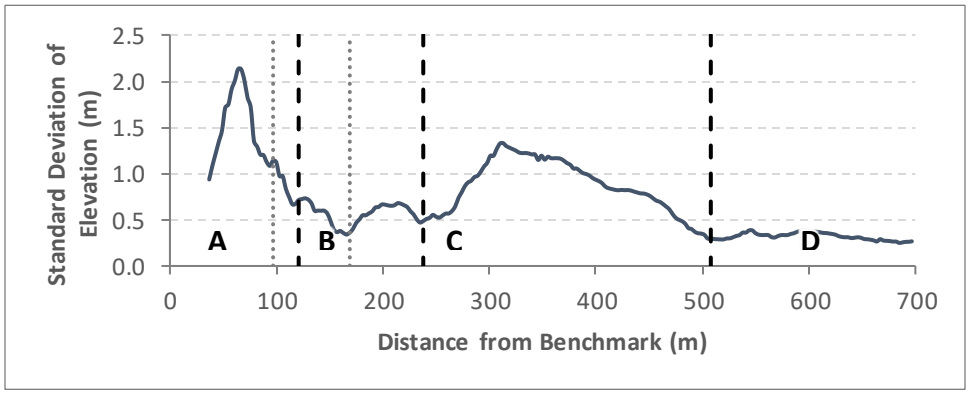

b) UM14

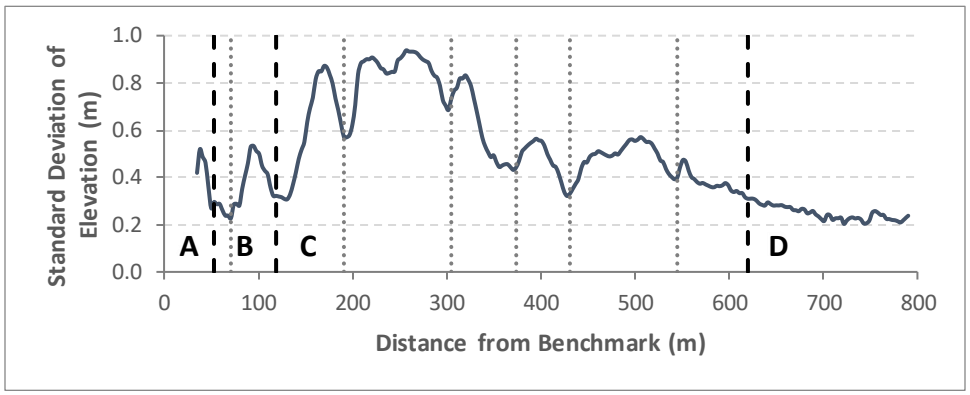

c) UM19

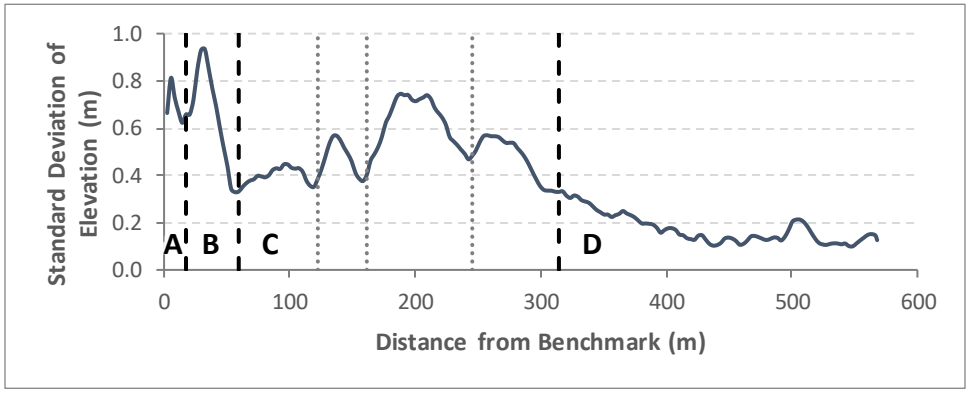

Sector Boundary Subsector Boundary

Figure 14. *Classification of cross-shore profile sectors based on standard deviations of profile elevations.* Figures display the sector and subsector boundaries identified at each study site. Sector boundaries are shown at nodes between the major profile morphological zones. Subsector boundaries are placed at smaller nodes which occur within major sectors before a transition to a different sector type.

Figure 14 (cont'd)

d) UM21

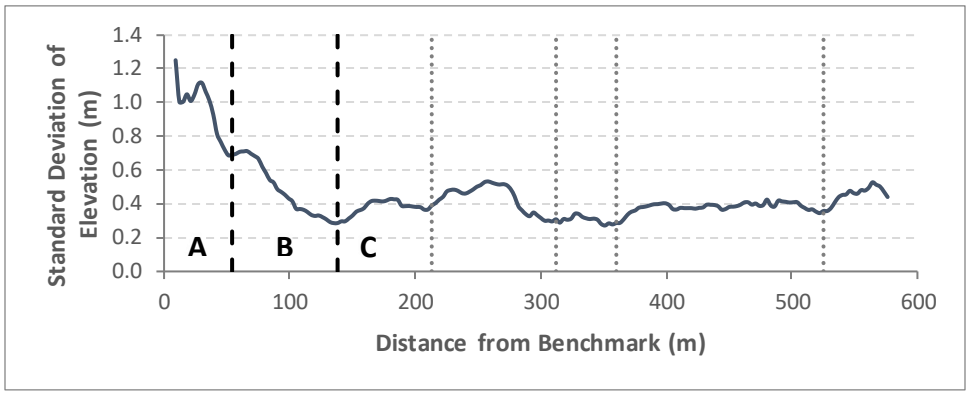

e) UM22

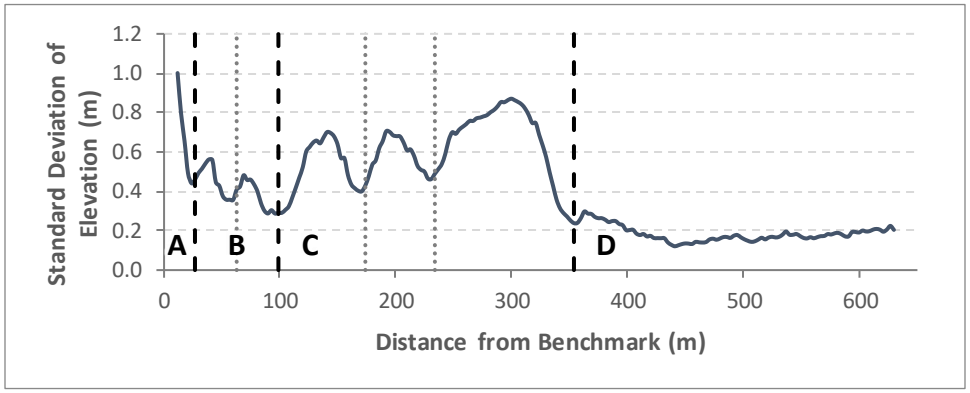

f) UM29

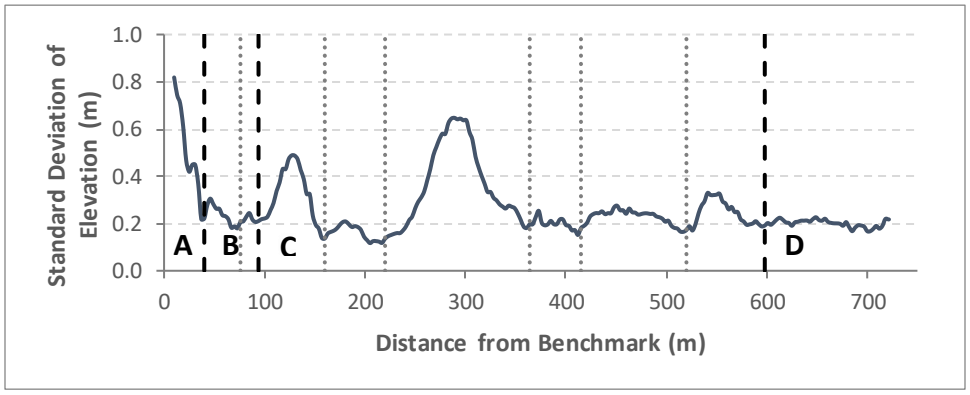

APPENDIX D: MEAN SEDIMENT MOBILIZATION LIKELIHOOD

a) UM04

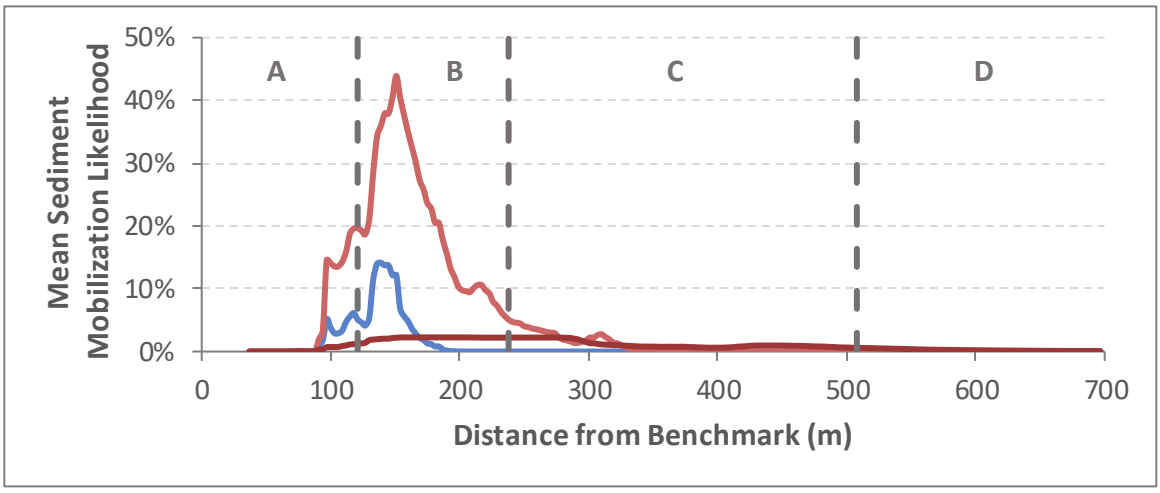

b) UM14

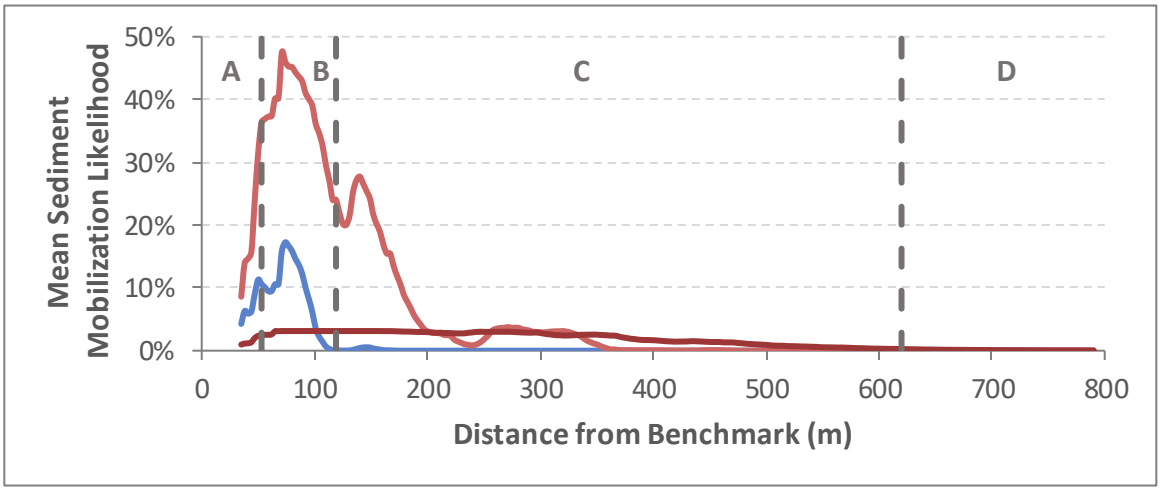

Figure 15. *Mean sediment mobilization likelihood across all study sites.* Figures display the mean sediment mobilization likelihood curves for AC, ME, and SE morphodynamic conditions for all six study sites. These likelihoods are calculated by averaging the amount of time each location along the surveyed coastal profile was within the active zone for sediment transport during each MC over each of the nine study periods. Overall, profile sectors A and B have the highest overall mobilization likelihoods, while ME conditions are the most common MC. AC mobilization likelihoods are highest in sectors A and B, indicating that onshore-directed sediment transport during conditions conducive to beach recovery likely mobilizes shallow sediments contained in these sectors.

Figure 15 (cont'd)

c) UM19

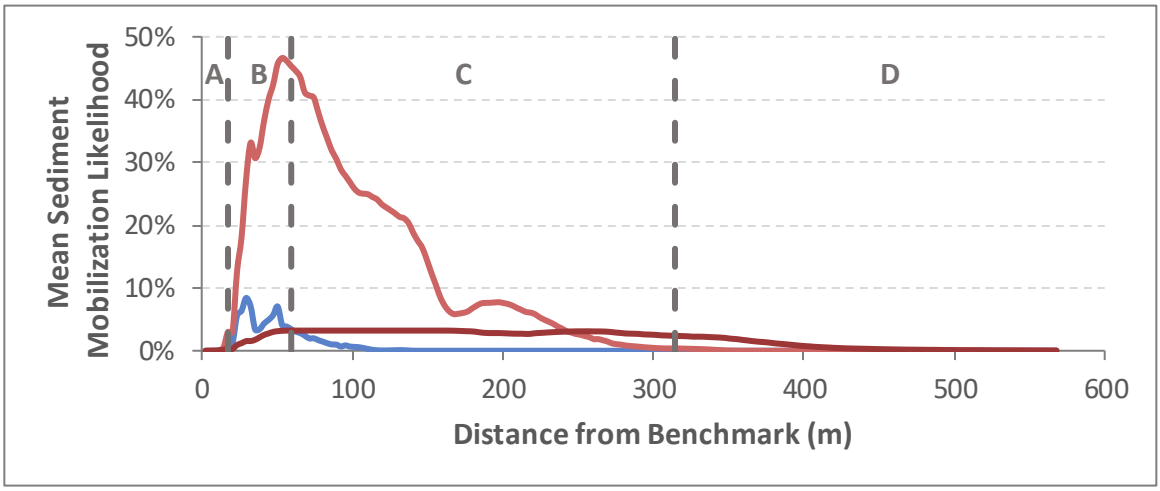

d) UM21

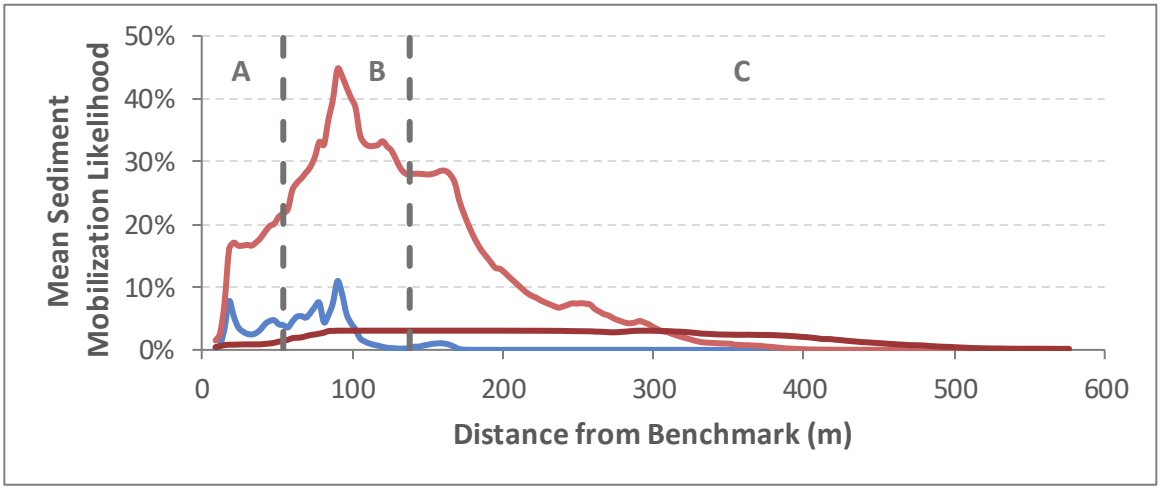

e) UM22

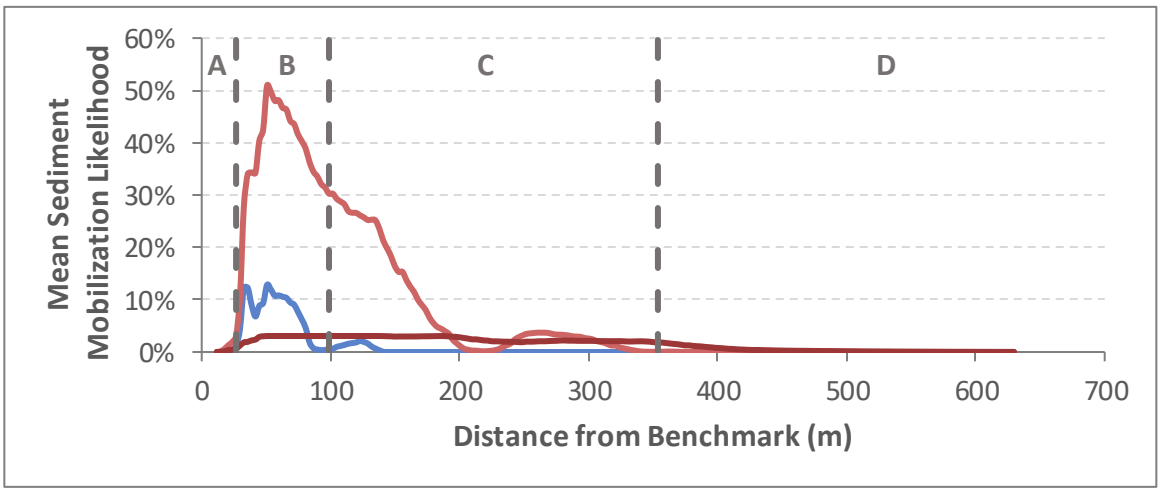

Figure 15 (cont'd)

f) UM29